# Chapter 9
# Landslide Inventory, Hazard and Risk Assessment in India

**Cees J. van Westen, Pankaj Jaiswal, Saibal Ghosh, Tapas R. Martha and Sekhar L. Kuriakose**

**Abstract** The recent census in India revealed that India is now housing 17% of the world's population, and India is on the way to become the most populated country. Landslides are an increasing concern in India due to the rapid population expansion in hilly and mountainous terrain. Landslides affect vast areas within India, in particular in the Himalayan chain in the North and Eastern part of the country and the Western Ghats in the Southwest. The Geological Survey of India (GSI) has been designated as the nodal agency for landslides by the Indian government, and they are responsible for landslide inventory, susceptibility and hazard assessment. Until recently their landslide susceptibility assessment was based on a heuristic approach using fixed weights or ranking of geofactors, based on guidelines of the Bureau of Indian Standards (BIS). However, this method is disputed as it doesn't provide accurate results. This paper gives an overview of recent research on how the existing methods for landslide inventory, susceptibility and hazard assessment in India could be improved, and how these could be used in (semi)quantitative risk assessment. Due to the unavailability of airphotos in large parts of India, satellite remote sensing data has become the standard data input for

C. J. van Westen (✉)
Faculty of Geo-Information Science and Earth Observation (ITC), University of Twente, Enschede, Netherlands
e-mail: westen@itc.nl

P. Jaiswal · S. Ghosh
Geological Survey of India, Kolkata, India

T. R. Martha
National Remote Sensing Center, Indian Space Research Organization, Hyderabad, India

S. L. Kuriakose
HVRA Cell, Department of Revenue and Disaster Management, Government of Kerala, Trivandrum, India
e-mail: sekhar.lk@gmail.com

B. Pradhan and M. Buchroithner (eds.), *Terrigenous Mass Movements*,
DOI: 10.1007/978-3-642-25495-6_9, 

landslide inventory mapping. The National Remote Sensing Center (NRSC) has developed an approach using semi-automatic image analysis algorithms that combine spectral, shape, texture, morphometric and contextual information derived from high resolution satellite data and DTMs for the preparation of new as well as historical landslide inventories. Also the use of existing information in the form of maintenance records, and other information to generate event-based landslide inventories is presented. Event-based landslide inventories are used to estimate the relation between temporal probability, landslide density and landslide size distribution. Landslide susceptibility methods can be subdivided in heuristic, statistical and deterministic methods. Examples are given on the use of these methods for different scales of analysis. For medium scales a method is presented to analyze the spatial association between landslides and causal factors, including those related to structural geology, to select the most appropriate spatial factors for different landslide types, and combine them using the multivariate methods. For transportation corridors a method is presented for quantitative hazard and risk assessment based on a landslide database. Deterministic methods using several dynamic slope-hydrology and slope stability models have been applied to evaluate the relation between land use changes and slope stability in a steep watershed. The paper ends with an overview how the susceptibility maps can be combined with the landslide databases to convert them into hazard maps which are subsequently used in (semi) quantitative risk assessment at different scales of analysis, and how the results can be used in risk reduction planning.

**Keywords** Landslide inventory · India · Historical landslide data · Object oriented image classification · Event-based landslide maps · Statistical analysis · Physical modeling · Hazard assessment · Risk assessment

## 9.1 Introduction

Landslides are an increasing concern in India due to the ongoing expansion of the population into hilly terrain (Kuriakose et al. 2009a). Vast areas within India, in particular the entire Himalayan chain in the North and Eastern part of the country and the Western Ghats in the Southwest are affected by landslides.

For instance, the densely populated state of Kerala in India is prone to debris flows due to its geomorphic setting as 40% of it lies in the most prominent orographic feature of peninsular India, The Western Ghats. The west facing scarps that runs the entire extent of the Western Ghats mountain chain in Kerala experience several types of landslides, of which shallow landslides and consequent debris flows are the most common (Kuriakose et al. 2009b). Many of the roads and railroads that run through the Himalayas and the Western Ghats (Jaiswal and van Westen 2009; Sreekumar 2009) are highly prone to landslides. Over the period of 1975–1995, it is estimated that landslides killed about 100 people and rendered about 600 families homeless along the Western Ghats (Thakur 1996) whilst floods

and landslides together have caused an estimated damage of 12 billion Euros in Kerala in 2007 alone (Murali Kumar 2007).

The Geological Survey of India (GSI) has been designated as the nodal agency for landslide studies by the Government of India. The GSI was established in 1851 though it was only in 1945 that the engineering geology and ground water division of GSI was created which had landslide investigation as one of its main responsibilities. Since its inception GSI has investigated many disastrous landslides, such as the Nainital landslide in 1880, the blockade of Birahi Ganga by a massive rockfall at Gohna in Garhwal in 1893, the Malpa landslide in 1998 and the Uttarkashi landslide in the 1990s', just to name a few.

Though there are several site specific studies, spatial landslide hazard and risk assessment in India has always been hampered by the lack of data. Along the international border regions of the country including the entire Himalayan range, the use of topographical maps and aerial photos has been restricted for national security reasons. Thus, for long the generation of landslide inventory maps faced significant lacuna. In lieu of aerial photos for large parts of the country, satellite remote sensing data has become the standard input for landslide mapping. The National Remote Sensing Center (NRSC) under the Indian Space Research Organisation (ISRO) has been very active in the use of satellite data for landslide inventory mapping and susceptibility assessment. High resolution stereo imagery from satellites such as Cartosat 1 has proven to be very useful for landslide studies (Vinod Kumar et al. 2006).

In 1998, the Bureau of Indian Standards (BIS) formulated guidelines for landslide susceptibility zonation on macro scale (1:50,000) for the whole country (BIS 1998). These guidelines propose an indirect approach to landslide susceptibility mapping based on a generalized heuristic system of fixed weighting or ranking of geofactors without directly or indirectly considering the landslide inventory data (Anbalagan 1992; Anbalagan and Singh 1996; Sarkar et al. 2008). Its' direct applicability in all the landslide prone regions of the country is a matter of dispute amongst landslide researchers owing to the wide variability of the geoclimatic conditions that prevails across the country.

Due to the difficulty in obtaining base maps and multi-temporal landslide inventory maps, the development of new approaches for landslide hazard and risk assessment, including the use of spatially distributed physically-based landslide initiation models, run-out models and statistical models, have always been impeded in India. In this paper we present the results of the application of some of these new techniques for landslide inventory, susceptibility mapping and, hazard and risk assessment as applied to four test sites in different regions of India.

## 9.2 Study Areas

Figure 9.1 shows the locations of the four test sites. Two of these are located in the Western Ghats and two in the Himalayas. The test site in Kerala (A in Fig. 9.1) is

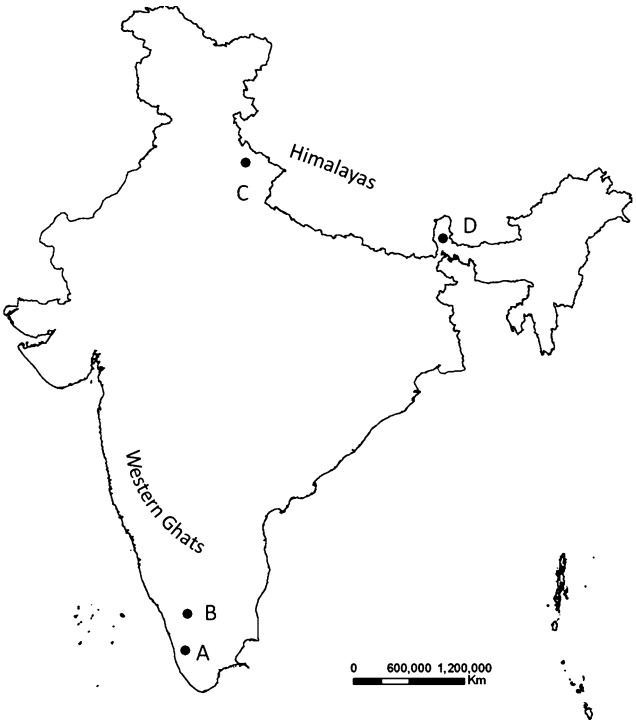


**Fig. 9.1** Location of the test sites in India. **a** Upper Meenachil River basin. **b** Nilgiri. **c** Okhimath. **d** Kurseong

the upper Meenachil River basin upstream of Erattupetta Town. The region is administratively part of Kottayam and Idukki districts (Fig. 9.2). The area experiences numerous shallow landslides leading to debris flows almost every year during the monsoon season. Two separate study areas (Fig. 9.2 ) namely Aruvikkal catchment and Peringalam landslide in the region were selected to test a physically based dynamic shallow landslide model and a run-out model, respectively. As per measurements at Pullikanam Tea Estate's Upper Division, which is the closest long term rainfall recording station, the region experienced an average annual rainfall of 5315 mm during the period from 1952 to 1999. Underlain by Precambrian charnockites the region is predominantly covered with shallow sandy soils over a thin layer of sparolite interleaved by lithomargic clay (Kuriakose et al. 2009c). Anthropogenic land disturbances in the area started in the late 1880s (Victor 1962). The predominant land use of the region is rubber plantations, covering an area 3.6 $km^2$. Rubber has an average crop life of 20 years after which the trees have to be felled, thus exposing the land to the high intensity rainfall until a new set of saplings are planted and they achieve significant canopy cover. Both for cassava and rubber planting, slopes are terraced often ignoring ephemeral streams thereby

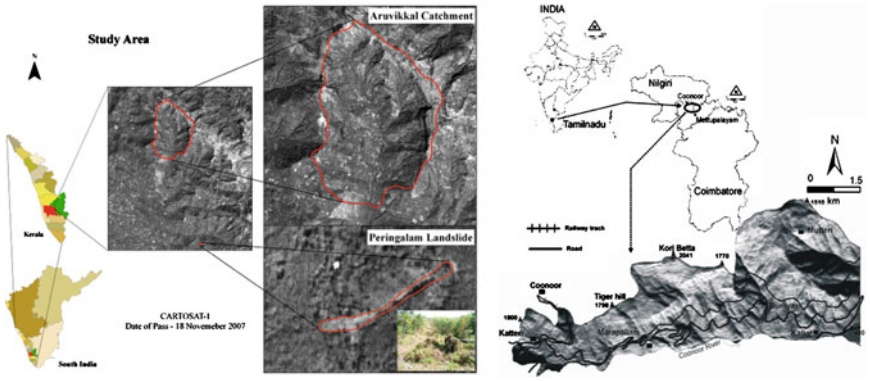


**Fig. 9.2** Study areas in the Western Ghats. *Left*: Aruvikkal catchment and Peringalam Landslide. *Right*: Nilgiri area

obstructing natural drainage channels that act as conduits for the discharge of excessive surface flow during high intensity rainfall (Thampi et al. 1998).

The second study area (B in Fig. 9.1) is located in Nilgiri (Tamil Nadu) and includes a 19 km long historic railway track, which is declared as a world heritage site by UNESCO and a 26 km long national highway connecting Mettupalayam and Coonoor in the state of Tamil Nadu in southern India (Fig. 9.2). The railway was constructed in the late nineteenth century and became operational in 1899. Both transportation lines run parallel to each other on the southern slopes of the Nilgiri plateau. The routes are cut through soil and laterite, underlain by charnockite and garnetiferrous quartzo-felspatic gneisses belonging to the Charnockite Group of Archaean age (Seshagiri and Badrinarayanan 1982). The regional strike of the foliation is ranging from ENE–WSW to E–W direction with moderate to steep dips. The sub-tropical climate and intense physical and chemical weathering have resulted in a thick yellowish to reddish brown soil. The regolith thickness varies from less than one meter to 20 m, as observed in the cut slopes along the road and railroad. The study area forms a part of the Nilgiri plateau with steep slopes to the south and gentle slopes to the north and near ridge tops. The area has an elevation difference of 1641 m with lowest areas near Kallar farm (400 m) and highest at Kori Betta ridge (2041 m). Most part of the transportation corridor is either under reserved forest or tea plantation and settlements are very few and sporadic. Landslides are abundant in the area and occur mostly in cut slopes of the transportation routes. These are mostly shallow translational debris slides and flows and are invariably triggered by rainfall (Jaiswal and van Westen 2009).

The third study area (C in Fig. 9.1) is a part of Mandakini river valley in the High Himalayas, located around the town of Okhimath in the Rudraprayag district of Uttarakhand state, India (Fig. 9.3). Okhimath is situated at an average elevation of 1300 m at the confluence of the Mandakini and Madhyamaheshwar rivers. The Mandakini River is a tributary of the Ganges River. The region has a highly variable land cover and terrain with elevation ranging from 718 to 4510 m.

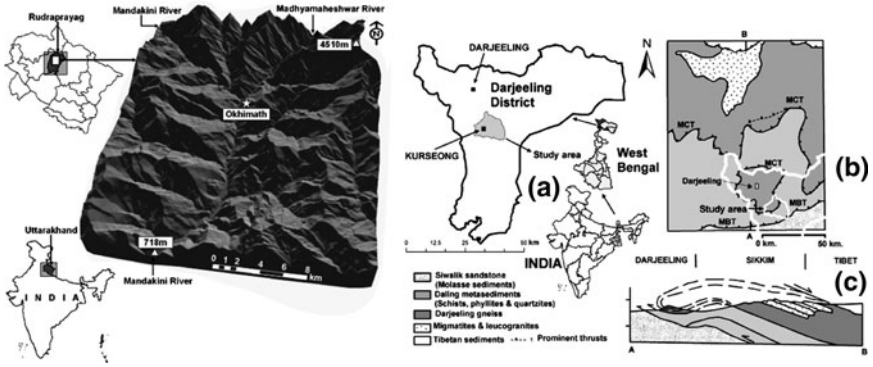


**Fig. 9.3** Study areas in the Himalayas. *Left* Okhimath. *Right* Kurseong

The northeastern part of the area is perennially snow covered. This area is dominated by low altitude oak forest. The terrain is dominantly steep and rugged with few flat fluvial terrace areas along the Mandakini River. Since the rugged topography is controlled by the geological structure, there are many fault-related south facing escarpments in this area. The northeastern and western parts of the area are very difficult to access.

The fourth study area (D in Fig. 9.1) is located in Darjeeling district, West Bengal, within the eastern part of the Himalayas (Fig. 9.3). The eastern Himalayas represent a complicated geological and tectonic environment, in which rocks are juxtaposed along certain E–W trending Tertiary regional thrusts. Along the foothills to the south, coarse to very coarse-grained clastics (conglomerate-sandstone–siltstone) of the so called Siwalik Group of Tertiary age are exposed and are bordered by a frontal thrust (Himalayan Foothill Thrust—HFT or Himalayan Frontal Thrust HFT). To the north these are thrusted over by sandstone-shale (±coal) sequence of the Gondwanas (Mesozoic) along the Main Boundary Thrust (MBT). Further to the north, low grade meta-psammo-pelitic lithoassemblages of the Precambrian Daling Group are thrusted over the Younger Gondwana/Siwalik sediments. And further north in the Middle to Higher Himalaya, granite gneisses and high-grade meta-sediments belonging to the Central Crystalline Gneissic Complex (CCGC) are thrusted over the low-grade metamorphics of the Daling Group along the Main Central Thrust (MCT). The overall relief difference in the studied area varies from 250 m to as high as 2650 m. The general trend of the mountain ranges is E–W. A number of NE–SW and NW–SE trending ridges and spurs are carved out of this trend and form high mountain ranges. The average rainfall in Darjeeling Himalaya to the west of the Tista River fluctuates between 2000 mm and 4000 mm. Landslides are perennial problems in Darjeeling Himalayas during monsoon (June to October) resulting in frequent closures of important communication corridors, destruction of limitedly-available agricultural land, house and loss of human life. The earliest recorded landslide event in Darjeeling Himalayas, India dates back on 24th September 1899, which was triggered by a 1065 mm precipitation (in 3 days) and resulted in devastation in Darjeeling town and

its surrounding areas with loss of 72 lives. Since then, this part of the Himalayas has experienced such comparable devastating landslide events in at least 10 times till 2003, although the intensity and distribution may differ considerably for individual extreme rainfall events.

## 9.3 Landslide Inventory Mapping

Landslides are generally isolated natural processes, which individually may not be of very large in size but can occur with a high frequency in an area (van Westen et al. 2006). Landslide inventories can be prepared through various methods (Guzzetti et al. 2000; Hansen 1984; van Westen et al. 2008; Wieczorek 1984) such as historical archive studies, interviews, detailed geomorphologic fieldwork, and mapping from remote sensing data and topographic maps. Each of the methods indicated above has its drawbacks. Due to the lack of sufficient historical information on landslides, stereoscopic interpretation of aerial photographs or satellite images from the past is often used as the main source for obtaining a multi-temporal landslide inventory (Rib and Liang 1978). Event-based inventories are prepared just after a prominent triggering event which depicts all slope failures caused due to that particular triggering event (Carro et al. 2003; Guzzetti et al. 2004; Harp and Jibson 1996).

A landslide inventory contains the location, classification, volume, run-out distance, date of occurrence and other characteristics of landslides in an area (Fell et al. 2008). Techniques used to prepare landslide inventory maps depend on the quality and accessibility of desired information, the scope and the extent of the study area, the scales of base maps and the resources available to carry out the work. In this case study an approach is presented to obtain a complete multi-temporal landslide inventory by interpreting historical records coupled with participatory mapping. There are different techniques for landslide inventory mapping, three of which are illustrated in the following sections: using historical data, image interpretation and automatic classification.

### *9.3.1 Collecting Historical Landslide Information*

In the Nilgiri area (B in Fig. 9.1) it was possible to generate a very detailed landslide inventory based on historical data. The data sources used to obtain landslide information can be grouped into three main categories:

- *Railroad maintenance records* such as the railroad maintenance registers (locally called ‘railway slip register’) and a summary table of landslides along the railroad. The data were present in an analog (paper) form recorded in a register or table and maintained by the Southern Railway office at Coonoor. The railway

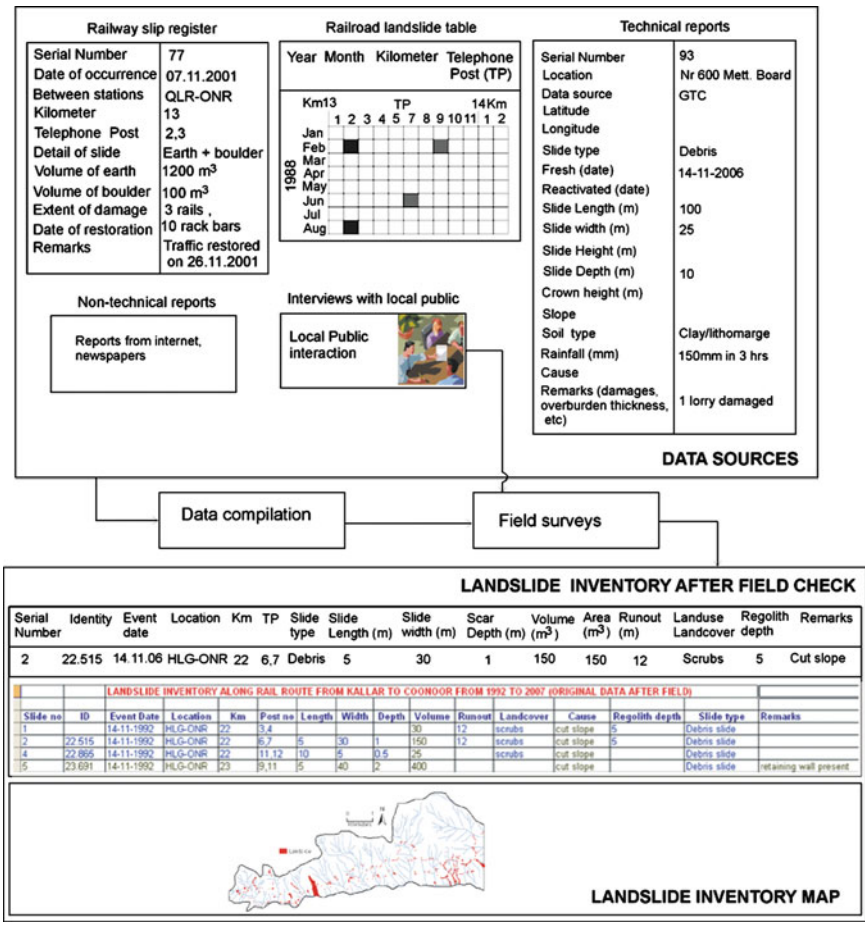


**Fig. 9.4** Different types of data sources and methodology used to prepare landslide inventory

slips register is updated soon after the occurrence of a landslide triggering event and is used for tendering contracts for railroad clearance. It contains data on the spatial distribution of landslide debris on the railroad for the period since 1992. The other form of historical records was a summary table of landslides along the railroad, which provided the spatial distribution of debris on the railroad in different months and sectors from 1987 to 1991. Landslides prior to 1987 were also recorded in the form of a landslide table but for the study area older records were not available in the railway office. The data format and an example of the type of data available in the records are shown in Fig. 9.4. The records also provide additional information on damages and the date of restoration of the railroad for traffic.

- *Technical reports* such as published and unpublished technical documents of landslide investigations. Publications on landslides in the Nilgiri area

(e.g., Seshagiri et al. 1982; Ramasamy et al. 2003) provided detailed information including the spatial distribution of the landslides during the major events in 1978 and 1979. In the unpublished technical reports the oldest information on landslides dates back to 1824. Most of the reports contain information on detailed geotechnical investigation of the major landslides that have occurred in the Nilgiri area. Besides, they also contain inventory of landslides that have affected the road in the period since 1987. Before 1987, no systematic record of landslides along the road is available with the technical offices. The data format and type of information extracted from the technical reports along with an example is shown in Fig. 9.4.

- *Non-technical sources* such as internet (NDM 2009), newspapers, and interviews with local people. They provided additional information on the date of occurrence and damages caused by landslides. Interviews with local people have helped in estimating the indirect economic loss resulting from road blockages.

The landslide characteristics was compiled in standardized forms, and rearranged based on the location description. This data formed the basis for field mapping where all the landslide dates related to one specific location was listed in a tabular form. All landslide sites reported in the historic archives were visited and an attempt was made to identify the landslide scars. Some of the landslide scars and run-out areas were not clearly discernable due to the removal of debris and remedial works. During the field work, local residents were interviewed and questions were asked pertaining to their livelihood, and any information regarding landslides and damages. For example, during the field mapping, an old worker from the railway office has helped in locating older landslides based on the clearance work that he had carried out. After identifying the exact location of a landslide it was then mapped on a 1:10,000 scale topographic map and its initiation (source) and run-out area were separately marked. The morphological parameters were plotted after measuring them in the field. Additional data such as type of landslide, run-out distance, present land use and land cover, probable cause, regolith thickness, and damage details were also added to the inventory. The mapped landslides were digitized as polygons or points and entered in a geo-database of ArcGIS. Separate layers were prepared for the landslides associated with cut slopes and natural slopes. The smaller landslides were digitized as points in a separate layer. A unique identification number (ID) was assigned to each landslide (polygon or point), which provided a link between the spatial and non-spatial attributes.

In total 1040 landslides were compiled from the historical records and field work within a 22 $km^2$ area. The inventory was nearly complete for the period 1987–2007. Landslides were triggered on 116 different dates. From the total of 1040 landslides, 643 landslides (62%) were obtained from the railway slips register, 259 (24%) from the landslide summary table along the railroad, 132 from technical reports and six from the other sources. Through field mapping it was possible to identify 67% of the compiled landslides. Some of the smaller landslides were not identifiable in the field due to possible reactivations which have obliterated the earlier morphology. The volume of these small landslides was therefore

taken directly from the original source data. Since they were small and located along the road or the railroad, it was presumed that most of the released material from these landslides was accumulated on the road and the railroad. Therefore, the measured volume from the maintenance records was considered a good representation of the size of these landslides. Landslides were classified as debris slide and debris flowslide following the classification proposed by Cruden and Varnes (1996). Landslides initiating as slide and then converting to flow under saturated condition were grouped under 'debris flowslide'. About 97% of the landslides were debris slides. Most of these were shallow translational with a depth of the slip plane less than 5 m. Only three landslides were found to have a depth of more than 5 m. The landslides are further regrouped into cut slope and natural slope failures based on the location of their source area. Most of the landslides (96%) were recorded in cut slopes. Smaller landslides in the cut slopes were found to have a short run-out as the road and the railroad acts as a platform for the accumulation of the debris. In terms of the volume of material displaced, most of these landslides (91%) lie within the range of 2–500 $m^3$.

The landslide distribution map is shown in Fig. 9.5. At some places (e.g., Fig. 9.5b) the railroad has cut slopes on both sides. The cut slopes on the valley side act as a barrier and prevent landslide debris moving downslope. All the debris falling from the slopes accumulates on the railroad. The annual distribution of recorded landslides in the past 21 years is shown in Fig. 9.5e. Landslides occur annually in the area (except in 1995) with an average rate of 20 landslides per year. At some locations the same slope is affected by landslides in different periods (e.g., Fig. 9.5c, d). On November 14, 2006 about 205 landslides occurred mostly in the eastern part of the area. This occurrence corresponds to high intensity rainfall (150 mm rainfall in 3 h). In terms of the monthly distribution of recorded landslides, November is the severest month (Fig. 9.5f) containing 58% of the landslides. This month also receives the highest rainfall each year due to the retreating monsoon.

Interpretation of historical data pertaining to the Nilgiri area was carried out for generating a complete multi-temporal landslide inventory. An inventory remains incomplete when location references of landslides are not available, and in most cases features left by landslides cannot be recognized in the field or through the interpretation of aerial photographs, as they are often obscured by erosion, vegetation and human interferences. In literature there is no unique measure of completeness of an inventory, but if an inventory is prepared soon after the triggering event then there is a greater possibility of recording all landslides in an area. For the study area a similar inventory was available in the form of a railroad maintenance archive. It is updated soon after the occurrence of a landslide triggering event and is used for tendering contracts for railroad clearance. Completeness of an inventory can also be tested by studying the magnitude-frequency relation of landslides. In most cases, the structure of the magnitude-frequency relationships were found to have a power law distribution over two orders of magnitude (landslide area) with a flattening of the curve at lower magnitudes, termed as 'rollover'. This rollover or less frequent occurrence of smaller landslides

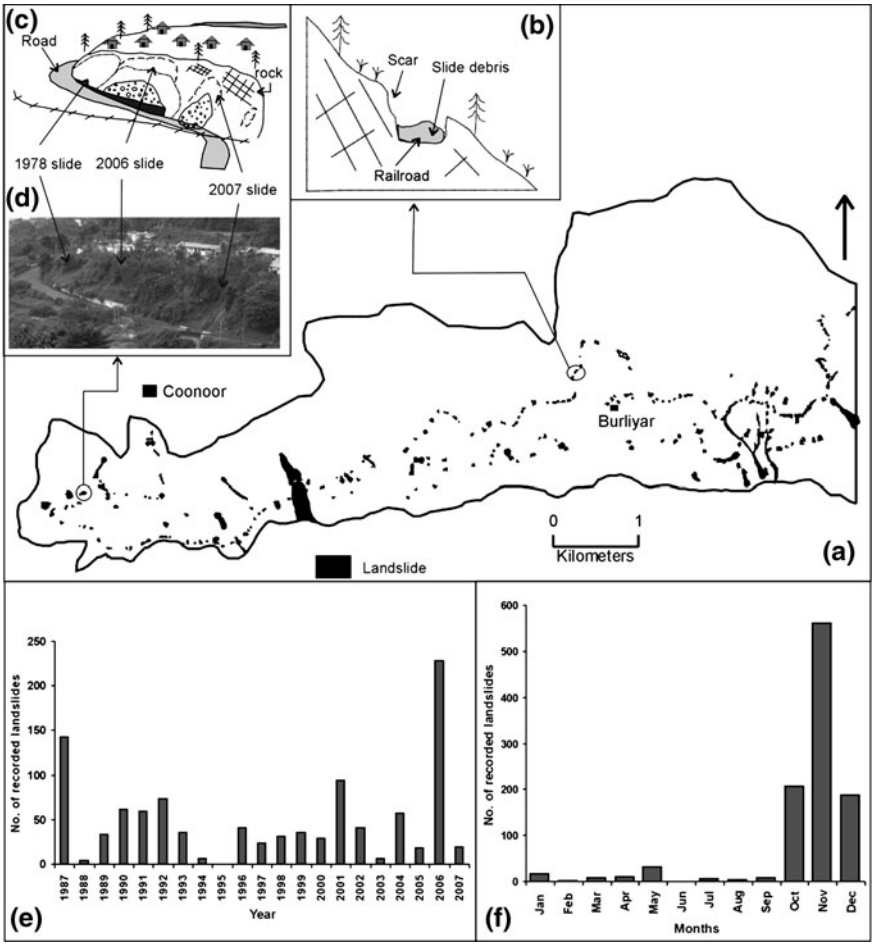


**Fig. 9.5** **a** Landslide inventory map. **b** Sketch of the railway having cuts lopes on both sides. **c** Sketch showing landslides in different years in one slope. **d** Field photograph of landslides in cut slope at Katteri. **e** Distribution of landslides over the past 21 years. **f** Annual distribution of landslides

is debated as a real effect reflecting slope stability processes (Guthrie and Evans 2004) or due to the incompleteness of the inventory (Malamud et al. 2004). For the study area magnitude-frequency analysis was also performed and the structure showed a power law distribution with $\beta$ equals $-1.6259$ for all landslides with volume ranging from two to more than 104 $m^3$. For the same dataset, the probability distribution for landslide area also showed power law structure with $\beta$ equals $-1.6764$. The power function obtained from this study did not show any rollover effect, implying that the inventory did not suffer from the under-sampling of small landslides and thus is practically complete (Catani et al. 2005; Malamud et al. 2004).

### 9.3.2 Mapping Landslides from Multi-Temporal Images

In order to be able to express the spatial and temporal probability of landslides in regional hazard maps, it is important to know the location characteristics of the landslides and their behavior through time. One of the techniques used to generate such maps following a combined heuristic/statistical method is to generate multi-temporal landslide maps, linking the landslides to triggering events and use the temporal probability of the event in the hazard assessment combined with the spatial probability resulting from the statistical analysis. The success of generating event-based multi-temporal landslide inventories through stereoscopic interpretation of images/aerial photographs from different time periods depends on several factors. First of all the terrain characteristics, combined with the types and volume of landslides determine the period over which landslides that have occurred will still be recognizable in imagery of a later date. For instance, landslide will quickly become obliterated by vegetation in tropical environments, requiring many images with short time intervals in order to be able to map them. Secondly, the relation between triggering events, such as rainfall or earthquakes, and the landslides caused by these, can only be mapped if imagery is taken shortly after the triggering event. Thirdly the image interpretation skills of the geoscientists that make the image interpretation are important. Although well-trained and experienced geoscientists can make a good interpretation of recent landslides, they will have more difficulty in characterizing old and dormant ones (Carrara 1993). Errors in estimating the dimensions of landslides do exist due to inaccurate base maps (Malamud et al. 2004). Through time, multiple small slope failures may merge into larger landslides causing problems in the analysis of the frequency–magnitude statistics of landslides. Furthermore, for many of the mapped landslides, the exact date of occurrence remains unknown, thus making it difficult to relate such landslides with triggering events, especially as different landslide types have different relations with the meteorological triggers. In some situation, the post-event maps were even not prepared or no detailed information on such event-based landslides is available. The lack of such temporal information (exact date of occurrence) in landslide inventories, and incompleteness of past landslide information adds to serious bottlenecks in the determination of temporal probability and therefore pose difficulties in quantitative hazard assessment (van Westen et al. 2006).

The landslides were mapped using various data sources of 1968–2007 in a highly landslide-prone area around Kurseong in Darjeeling Himalaya, India (D in Fig. 9.1). The first step of generation of a multi-temporal landslide inventory was the collection of all available data on past landslide occurrences, such as, spatial data from high resolution satellite images, topographic sheets, old landslide maps and reports of field investigations and old aerial photographs. For this study, the oldest available data was of 1968. In that year, a major rainfall event occurred in Darjeeling Himalaya between 2 and 5 October with an amount of 1100 mm in 3 days, which caused a large number of landslides in different parts of Darjeeling

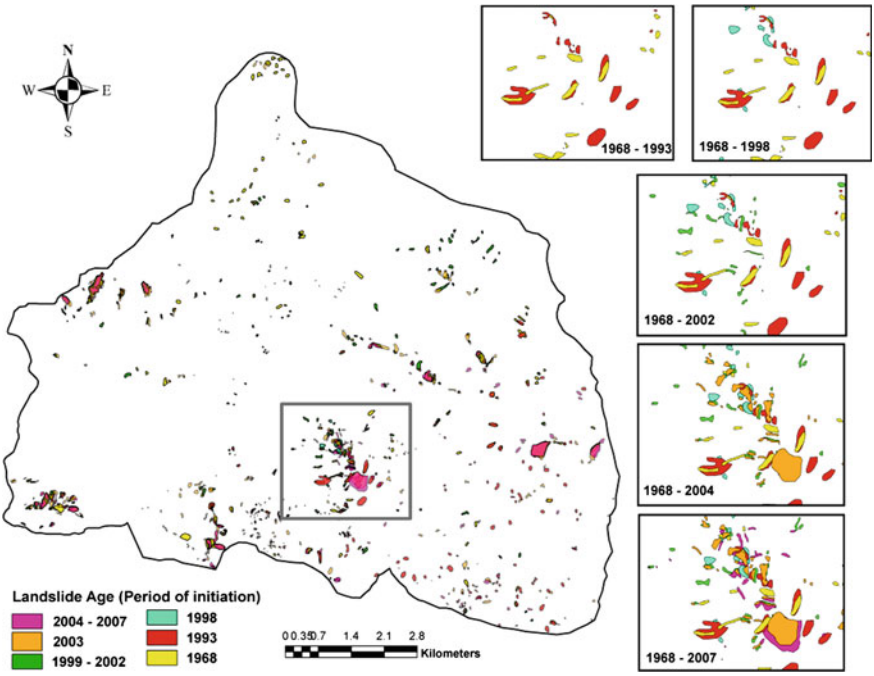


**Fig. 9.6** Multi-temporal landslide inventory map of Kurseong area, Darjeeling Himalaya, India

Himalayas (Basu and De 2003). During 1969–70, just after the event of 1968, the Survey of India (SOI) updated their topographic survey and prepared new 1:25,000 topographic maps. In these topographic maps, the locations of prominent and active landslides from 1968 were included. The next available data source is a field-based landslide inventory map of 1993 prepared by the Geological Survey of India (GSI) just after a landslide event that happened between 1 and 3 July, 1993 (Sengupta 1995). Unfortunately the field map of 1993 only covered the south-eastern part of the study area (56 $km^2$). The third data source represents another event-based landslide inventory map prepared by the Geological Survey through field investigations just after a prominent landslide event occurring between 6 and 8 July, 1998. Also this landslide inventory map covers only a part (central portion $\sim$20 $km^2$) of the entire study area, along a major communication corridor (NH-55) and around Kurseong town (Bhattacharya et al. 1998). Apart from these maps, high resolution satellite images namely, IRS 1D-PAN merged LISS III image (5.8 m resolution) of 2002, IRS P6-LISS IV MX image (5.8 m resolution) of 2004 and Cartosat 1 stereo pair (2.5 m resolution) of 2006 were also available. These were used together with a digital elevation model to produce stereoscopic images that were interpreted visually to map the landslide incidences from each set of imagery. The last data source used was a detailed fieldwork carried out in 2007,

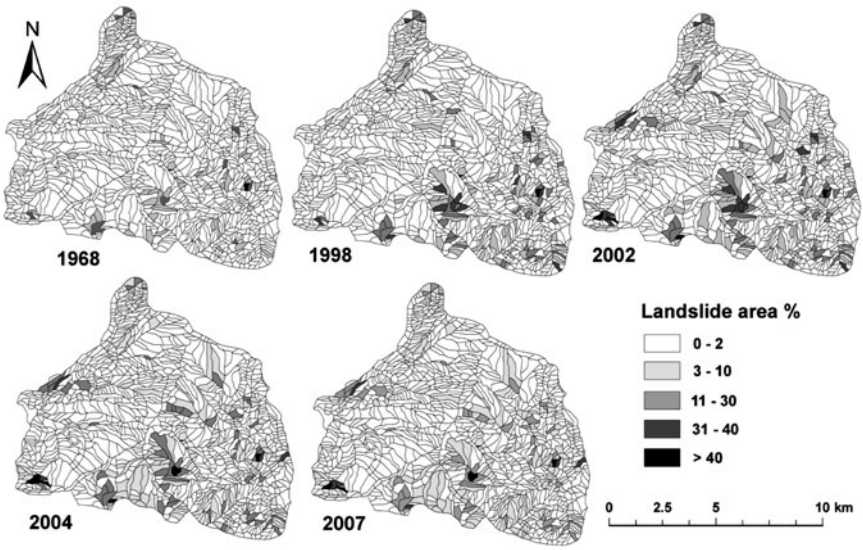


**Fig. 9.7** Spatio-temporal variation of landslide area percentage from 1968 to 2007

which allowed distinguishing the landslides that happened as a result of a rainfall event in 2007. Apart from the 1968, 1993, 1998, 2003 and 2007 event landslides, none of the data sources contained information on the exact dates of the landslide events, and thus, for some inventory maps; we could only attach a time period and not an exact date or year of the event.

All the spatial data were projected to UTM; WGS 84; 45N and the landslides were digitized as polygons. The landslides mapped were further updated and verified through extensive field observations in 2007–2008. During the field investigation in 2007 a more recent, post-event (July and September 2007) landslide map was prepared and added to the inventory database. The resulting map is shown in Fig. 9.6.

Despite constraints in the source database and the resultant inventories, we could compare in a GIS, the spatial locations of landslides of different time periods to know the frequency and pattern of new and reactivated landslides. Apart from the above, an analysis of landslide area percentage within different topographic slope units using inventories of different periods can also be observed to study the spatio-temporal changes in landslide distribution (Fig. 9.7). This inventory database can also suitably be used for the quantitative hazard analysis through identification of the recurrence interval of triggering events through multivariate modeling (Ghosh et al. 2009a) and by quantitative prediction of the probability of occurrences of landslides of different dimensions.

### 9.3.3 Automatic Landslide Mapping from Satellite Images

Aerial photo interpretation and field investigation are the traditional techniques for landslide mapping. Stereo-images are not only useful for the derivation of height information but also for landslide inventory mapping as it provides a 3-dimensional visualization opportunity. With the availability of high quality data products from new generation high resolution satellites and advancement in image processing techniques, satellite images are being increasingly used for landslide mapping. The main advantages of landslide mapping from remote sensing images are the synopticity, repetivity and sensor agility. The multi temporal images can be used to prepare a landslide activity map.

Based on the landslide diagnostic criteria, an expert prepares landslide inventory map from remote sensing images by visual interpretation. These diagnostic criteria can be effectively incorporated in a pixel or object based classification technique to automatically detect landslides. This helps in getting the result faster and the methodology is repeatable. Other remote sensing approaches of landslide inventory mapping include shaded relief images produced from Light Detection and Ranging (LiDAR) DEM and Synthetic Aperture Radar (SAR) interferometry. Detection of landslides include recognition and classification (Mantovani et al. 1996). One of the common methods in automated landslide mapping is change detection. In this method, time series data of an area are analysed to detect any change in the state of a matter e.g., landslide. Seven different categories of change detection techniques, their application and selection of the most suitable method have been summarized by Lu et al. (2004). Although difficult, spectrally similar matters such as bare rock and soil were successfully differentiated from landslides using the Maximum Likelihood Classification (MLC) method by Nichol and Wong (2005) using medium resolution SPOT data. Landslide crowns and trails as small as 7–10 m width were detected in the SPOT change images, and 70% classification accuracy achieved compared with an existing landslide inventory in the area. This method holds well if there is a clear spectral heterogeneity between landslide and its' surroundings e.g., landslides occurring in woodland. Merging of multispectral data with better resolution panchromatic data using image fusion techniques enhances the interpretability of the image and enables mapping of small landslides. Nichol and Wong (2005) applied different image fusion techniques to IKONOS data and found that PAN sharpening technique provides the best result and the fused image is useful for mapping very small landslides.

To overcome the limitations of pixel based methods, other researchers have attempted to use a combination of both satellite imagery and digital elevation models (DEMs) (e.g., Giles and Franklin 1998; McDermid and Franklin 1994). McDermid and Franklin (1994) noted that, in many cases, per pixel reflectance patterns are unrelated to geomorphic processes, and that classification schemes based on these data would fail. They suggested that a combination of geomorphometric criteria as well as spectral data would yield better results in identifying mass movement features. The automated landslide inventory mapping by image

segmentation technique using high resolution satellite data and DEMs will not only save time but also add a new dimension in further refinement of hazard assessment techniques by rapidly mapping the inventories after any triggering event on routine basis. Image segmentation is a preliminary step in object-oriented image classification that divides the image pixels into homogeneous, contiguous objects based on scale, colour, shape, compactness and smoothness. Object-oriented classification was introduced in the 1970s (De Kok et al. 1999). The initial application was limited by hardware, software, poor resolution of images and interpretation theories (Flanders et al. 2003). Since the mid-1990s, with an increase in hardware capability and availability of high spatial resolution images, the demand for object-oriented analysis has also increased (De Kok et al. 1999). Object based classification is superior to per-pixel classification (Blaschke and Strobl 2001). Segmentation of pixels into objects provides opportunity to apply geographical and morphological concepts to subsequent image processing such as classification. Thus it provides an information rich environment to work within any application domain. Object-oriented classification is potentially of great value in the detection of landslide scars because it allows spatial characteristics, such as the length to width ratio, to be included as class discriminators. So far the image segmentation approach has been restricted to landslides larger than 1 ha due to limitations in spatial resolution (Barlow et al. 2003). But with the availability high resolution satellite data (Table 9.1) there is a scope to identify even smaller landslides (100 $m^2$). The recognition and classification of individual process types (Cruden and Varnes 1996) using an automated approach has been less successful (Barlow et al. 2003). However, this limitation can be overcome by the use of curvature from DTM in the object based classification. Initially, spectral information with a suitable scale parameter was used to segment an image which produced image objects adequate to define the landslide boundary (Fig. 9.8). NDVI was used to separate landslides and its false positives from others. Subsequently, using morphometric parameters such as slope and flow direction, shape parameters such as compactness and asymmetry, and spectral parameters such as layer mean and ratios, the false positives were sequentially eliminated (Fig. 9.8a) and the remaining are the landslides. Based on the adjacency conditions such as high relative border to rocky land or weathered zone, a landslide was classified as a rock slide or debris slide, respectively. After landslides were classified based on material, the landslide objects were resegmented using the curvature data (Fig. 9.8c). A positive value for curvature indicates that landslide surface was convex upwards and negative value indicates that it was concave upwards. These criteria were used to classify landslides on the basis of the failure mechanism i.e. rotational and translational. Thus, using the object based classification method landslides were recognized and classified from remote sensing data and DEM.

The initial results indicate that a combination of high resolution satellite data and DEM is useful to prepare a landslide inventory map automatically. Object based detection is more promising in comparison to pixel based detection of landslides. This method is very helpful for rapid damage assessment and decision making process.

**Table 9.1** Landslide magnitude class for debris slide and debris slide/flow

| Magnitude class | Landslide type | Occurrence probability | Criteria used to define magnitude | |
|---|---|---|---|---|
| | | | Characteristic features | Damages and human perception |
| I | Slide | 0.722 | Shallow translational slides associated with cut/fill slopes; volume <100 $m^3$; scar depth <1 m; occur instantly; short run-out <10 m; depth of accumulated mass ~1 m; very high occurrence probability. | Minor or no damage to infrastructure (e.g., road or railroad or house); one can escape unhurt; controlled using simple retaining structures (e.g., retaining wall) |
| II | Slide and flow | 0.248 | Shallow translational slides associated with cut or natural slopes; volume of 102–103 $m^3$; scar depth <2 m; occur instantly as a single slide or more from a single cutslope; run-out <50 m; depth of accumulated mass ~1.5 m; high occurrence probability. | No damage to tarmaced road but can damage rail and non-RCC structures, one can escape; injuries minor; society live with it and accept risk; controlled using specially designed retaining structures (e.g., retaining wall with soil nailing). |
| III | Slide and flow | 0.026 | Shallow or deep translational slides associated with natural slopes; volume of 103–104 $m^3$; scar depth <8 m; confined or unconfined high velocity flow; run-out (~200 m) up to gentle slopes and deposit as fan of depth ~5–8 m; low occurrence probability. | No major damage to tarmaced road but complete damage to rail and buildings; uprooting of trees along path of flow; scouring of channel; escape possible; injuries major or even death in some cases; society live with it and tolerate risk; controlled by specially designed retaining structures of high cost. |
| IV | Slide and flow | 0.002 | Deep translational slides associated with natural slopes; volume of 104–105 $m^3$; scar depth >8 m; confined or unconfined high velocity flow; run-out up to gentle slopes and deposit as fan of depth >5 m; very low occurrence probability. | Complete damage to rail, road and RCC structures; uprooting of trees along path of flow; deep scouring of channel; no reaction time and difficult to escape; intolerable risk; area declared unsafe; controlled by specially designed structures of very high cost. |
| V | Slide and flow | <0.002 | Deep translational slides associated with natural slopes; volume of >105 $m^3$; scar depth >20 m; confined or unconfined high velocity flow; run-out up to gentle slopes and deposit as fan of depth >10 m; minor slides may precede before the event; very rare event. | Catastrophic event; total damage of infrastructure and properties of all types; complete uprooting of trees along path of flow; deep scouring of channel leaving hollow topography behind; no reaction time and difficult to escape; devastation and death; complete resettlement to other places; no further settlements allowed; controlled by specially designed structures of extremely high cost. |

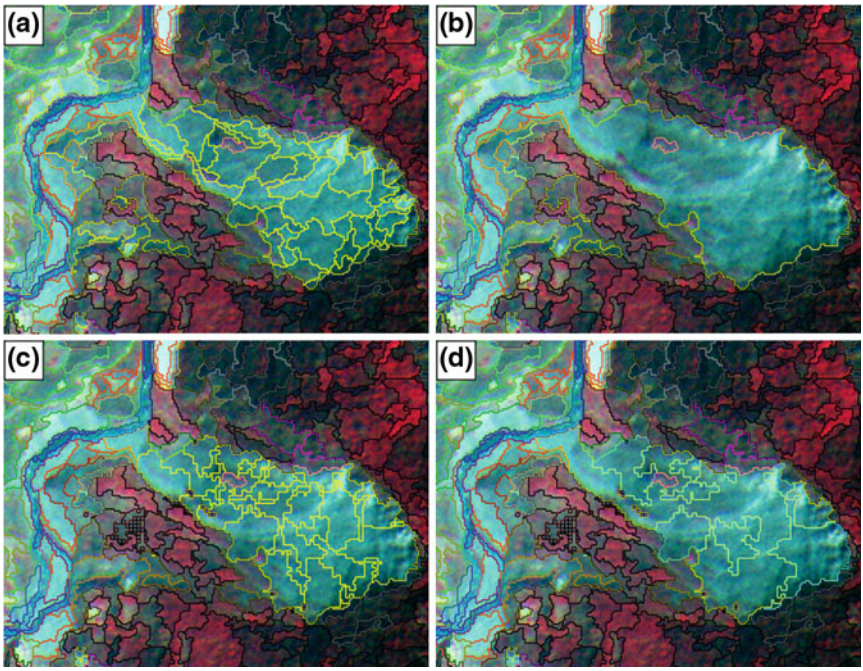


**Fig. 9.8** Results of image segmentation and object based classification for landslides using IRS-P6 LISS-IV Mx images and Cartosat-1 derived DTM. **a** Multiresolution segmentation with scale parameter as 10. *Yellow outline* shows landslides. **b** Landslide objec landslide objects classified based on material type and merged to give a single outline (*yellow colour*) to each landslide. **c** Resegmentation of landslide objects using curvature layer. **d** Classification of landslides using curvature value to rotational (*cyan outline*) and translational (*yellow outline*)

## 9.4 Landslide Hazard Assessment Approaches

Once landslide inventories have been made using one of the techniques presented above they can be used in different ways for landslide hazard assessment. In this section several methods are presented: direct hazard calculation based on complete landslide records, statistical analysis and dynamic modeling. An overview of the approaches and their applicability at different scales is given by Guidelines of the Technical Committee on landslides and Engineered Slopes, JTC-1 (Fell et al. 2008).

### *9.4.1 Direct Hazard Estimation Along Transportation Routes*

In this section we present the options that can be used to quantify landslide hazard if a complete inventory is available. Here we used the earlier described complete

multi-temporal landslide inventory prepared for the study area in Nilgiri hills (B in Fig. 9.1). Landslide hazard studies along a transportation line (road or railroad) focus on the landslides that may directly affect the infrastructure. The method requires assessment of two essential parameters:

1. The probability that a landslide affecting the infrastructure are of a given magnitude, and
2. The total number of landslides per kilometer affecting the infrastructure in a given return period.

In literature no established classification for landslide magnitude is available (Guzzetti et al. 2002). Some researchers have used landslide area or volume as a proxy for magnitude, for certain landslide types such as slides or flows (Guzzetti et al. 2005). In this study, a different landslide magnitude class is proposed. The landslides in the study area were grouped into five magnitude classes ranging from I (less severe) to V (catastrophic). The classification is essentially based on landslide type and volume, but it also addresses other characteristics such as the location of the source, damage potential and human perception about the risk related to landslides. The classification is semi-quantitative and derived on the basis of the historical information obtained during the inventory mapping (Table 9.1). The probability that a landslide affecting the infrastructure is of a given magnitude class was estimated using magnitude-frequency relationships. The probability was obtained from the probability density, for which a scatter plot was generated with landslide volume (in $m^3$) on the *x-axis* and probability density on the *y-axis*. The probability density function of landslide volume was found to have a good correlation with a power law distribution of type:

$$p(V_L) = k(V_L)^{-\beta} \tag{1}$$

where $k$ is a constant and $\beta$ is the power-law scaling exponent. Annual probability of landslide occurrence can be estimated from the observation of the frequency of past landslide events. The method generally used for estimating probability is by determining the annual exceedance probability (*AEP*), which is the estimated probability that an event will be exceeded in any year (Fell et al. 2005). The Poisson and Binomial distribution models are the two most commonly used models for such analysis (e.g., Coe et al. 2004; Guzzetti et al. 2005). The estimation of landslide risk, particularly indirect risk resulting from the blockage of transportation line, requires estimation of the number of landslides reaching the infrastructure per annum. The above model provides estimate of probability of experiencing one or more landslides and not the specific number of landslides. The number of landslides is required to calculate the blockage period based on clearance time needed per cubic meter of debris. The relation between the annual probability of occurrence of landslides (or return period) and the number of landslides of a magnitude class per kilometer can be established using a Gumbel extreme value distribution (Gumbel 1958).

For this study the annual probability was estimated from the total number of landslides per section of a transportation line in one year. The total number of landslides in a year per section of the transportation lines was selected from the inventory covering 21 years from 1987 to 2007. The yearly values were ranked from low to high, such that lowest rank 1 was assigned to the lowest data value and the highest rank 21 to the highest data value. At each section of the road and the railroad the expected number of landslides in 1, 3, 5, 15, 25 and 50 years return period were estimated. The Gumbel's distribution allows estimating the probability for return periods of 100 years or even more depending on the total length of the data. But, as a general rule, frequency analysis should be limited to expected events within a period twice the record length. In this study we estimated probability only up to 50 years return period, which is slightly more than twice the record length available for the study.

After obtaining all the relevant information such as the probability and magnitude of the landslide reaching the transportation line, the total number of landslides affecting the infrastructure in a given return period and its annual probability, the quantitative landslide hazard assessment was conducted for different sections of the transportation line. The landslide hazard, expressed as the number of landslides of a given magnitude per kilometer of the transportation line in a given return period, was calculated by multiplying the total number of landslides with the probability that the landslides are of a given of magnitude. The hazard estimation can be performed for a number of scenarios using different combination of landslide magnitude class and return period. For this study 24 scenarios were generated using four magnitude classes and six return periods.

Along the railroad Gumbel's analysis was carried out for segments of one kilometer thereby producing 19 Gumbel's plots for the total 19 km railroad. During the period from 1987 to 2007, the entire railroad was affected by 898 landslides of which the lowest was recorded in the vicinity of the kilometer stone number (ksn hereafter) 26 (14 landslides) and the highest around ksn-12 (101 landslides). During the same period the road was affected by 124 landslides with an average of 4.76 landslides per kilometer. The frequency of landslides in a year for different return intervals along the railroad line is shown in Fig. 9.9. A five kilometer stretch (from ksn-9 to ksn-13) is relatively more prone to be hit by landslides, as is the 10 km section (from ksn-390 to ksn-399) along the road.

Landslide hazard was estimated for 24 scenarios using the combination of four magnitude classes (class I–IV) and six return periods (1, 3, 5, 15, 25 and 50 years). An example of the scenario with 50 years return period along the railroad is given in Table 9.2. The results indicate that on an average once in 50 years (annual probability of 0.02) the entire railroad will be affected by 164, 56, 6, and 0.5 landslides of magnitude class I, II, III and IV, and the road by 5, 2, 0.2, 0.02 landslides of these classes.

The study showed that a direct landslide hazard assessment can be carried out if a complete landslide inventory is available. Hazard estimation in terms of number of landslides per kilometer and per year is possible only if the rate of occurrence of

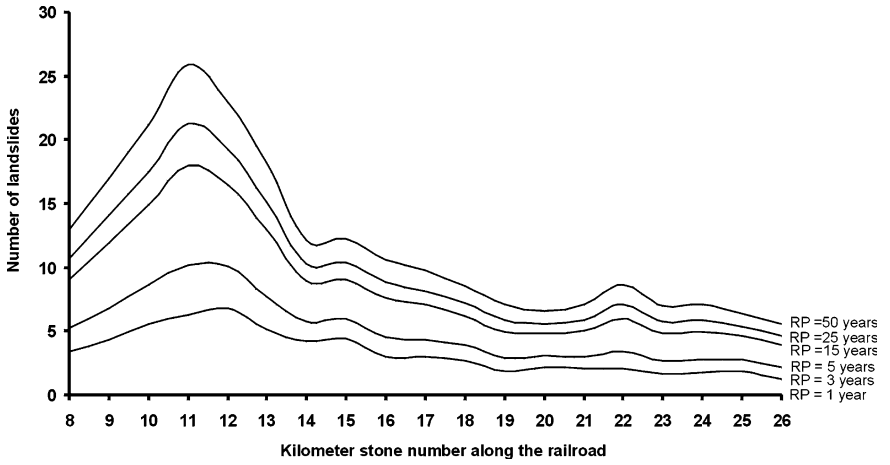


**Fig. 9.9** Frequency of landslides in a year for different return periods along the railroad

**Table 9.2** Landslide hazard along the railroad in 50 years return period

| Kilometer stone number | Total number of landslides of different magnitude class that can occur in a year | | | |
|---|---|---|---|---|
| km | I | II | III | IV |
| 8 | 9.31 | 3.20 | 0.34 | 0.03 |
| 9 | 12.25 | 4.21 | 0.44 | 0.03 |
| 10 | 15.26 | 5.24 | 0.55 | 0.04 |
| 11 | 18.68 | 6.42 | 0.67 | 0.05 |
| 12 | 16.56 | 5.69 | 0.60 | 0.05 |
| 13 | 13.15 | 4.52 | 0.47 | 0.04 |
| 14 | 8.79 | 3.02 | 0.32 | 0.02 |
| 15 | 8.82 | 3.03 | 0.32 | 0.02 |
| 16 | 7.67 | 2.64 | 0.28 | 0.02 |
| 17 | 7.03 | 2.42 | 0.25 | 0.02 |
| 18 | 6.14 | 2.11 | 0.22 | 0.02 |
| 19 | 5.09 | 1.75 | 0.18 | 0.01 |
| 20 | 4.74 | 1.63 | 0.17 | 0.01 |
| 21 | 5.10 | 1.75 | 0.18 | 0.01 |
| 22 | 6.22 | 2.14 | 0.22 | 0.02 |
| 23 | 5.03 | 1.73 | 0.18 | 0.01 |
| 24 | 5.10 | 1.75 | 0.18 | 0.01 |
| 25 | 4.62 | 1.59 | 0.17 | 0.01 |
| 26 | 4.01 | 1.38 | 0.14 | 0.01 |
| Total | 163.56 | 56.18 | 5.89 | 0.45 |

landslides is known and for such analysis continuous records of landslide incidences over a period of time is required. Any gap in the record may result in the over or underestimation of the probability. The Gumbel's distribution used in this

study is very appropriate in modeling extreme events such as incidences of large number of landslides. It helps in establishing a relation between the return period and number of landslides. The inclusion of the proposed magnitude class in the hazard assessment will help in analyzing the phenomena both in terms of risk to life and property. Ideally it should be quantified based on absolute values of landslide velocity, its intensity, its peak discharge, etc. But such parameters are very site specific and vary with local conditions such as channel geometry, terrain roughness, and land use, etc. and thus difficult to obtain and integrate in the hazard map. Due to this limitation and the complexity of landslide phenomena, the proposed classification is considered the most pragmatic solution. For the risk analysis, hazard assessment based on the number of landslides expected to hit per kilometer in a given return period is a workable solution. The assessment of direct and indirect risk becomes possible once the total volume of the expected landslide material is known.

### *9.4.2 Rock Failure Modeling Using Gis*

Many of the landslides in the Himalayas are rock slides, or are in weathering soil with a clear structural control. Structure represents nature and extent of discontinuity in the rock mass. For rock slides, since failure propagates along a near-planar surface (planar) or triggered along the intersection of two planes (wedge), presence/absence of any planar discontinuity, its nature, extent, orientation and frequency of occurrence in relation to topography are crucial deciding geofactors. The principle attributes considered in the rock structure are (i) blockiness or degree of rock dissection, (ii) geometric shape, orientation and form of the blocks and fragments and (iii) degree of looseness of the potentially unfavourable rock mass (Varnes and IAEG Commission on Landslides and other Mass-Movements 1984). Apart from the effect of predominance in the concentration of joints, faults and shears, locally, the geometric or kinematic interrelationships between the attitudes of bedding/foliation/joint planes and topography could be pivotal in deciding the mode of movement of rock slides (Briggs 1974; Günther et al. 2004; Hocking 1976; Hoek and Bray 1981; Meentemeyer and Moody 2000).

To determine the unfavourable *discontinuity-topography/structure domains,* we mapped different topographic segments after establishing the geometric interrelationships of the orientations between topography and prominent discontinuity surface following the classification proposed by Meentemeyer and Moody (2000). For the calculation of the angular interrelationship, raster maps of topographic slope (*S:* 0–90°), topographic aspect (*A:* 0–360°), discontinuity dip ($\theta$: 0–90°) and discontinuity dip direction ($\alpha$: 00–360°) were used. Slope and Aspect maps were directly derived from the 10 m $\times$ 10 m DEM. Dip and dip direction raster maps of prominent discontinuities were generated through interpolation (Inverse Distance Weighted) of discrete dip/dip direction values of foliation planes, measured at different point locations. After this, *structure domains* (Fig. 9.10) were derived by

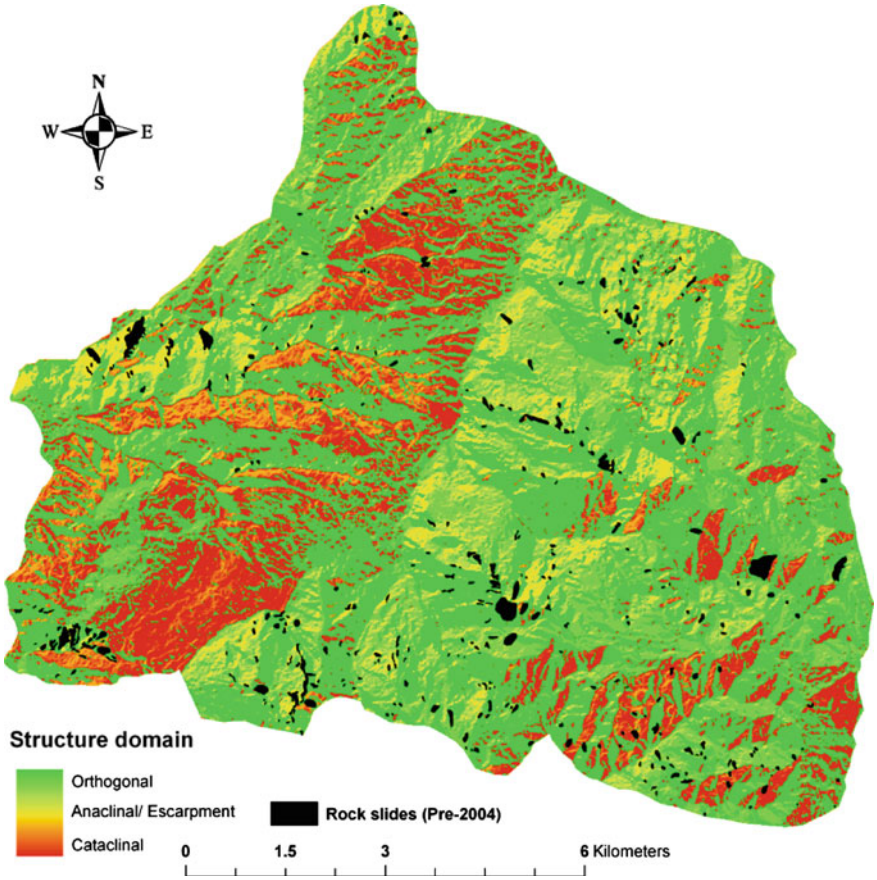


**Fig. 9.10** Map showing different structure domains of Kurseong (D in Fig. 9.1)

combining the above four raster maps and calculating their angular relationships. This map can be used as a predictor maps in susceptibility assessment.

Different rock slide failure mechanisms can also be successfully identified spatially by studying the kinematic interrelationships between the attitudes of distributed bedding/foliation/joint planes and topography through spatial correlation (Günther et al. 2004), which follows the criterion suggested by Hoek and Bray (1981).

The RSS-GIS extension of ArcView® 3.X is one of the very few software capable of automated spatial analysis with distributed rock structure data in a GIS platform (Günther 2005). This package was applied in the Kurseong study area (D in Fig. 9.11) to delineate the wedge and planar failure modes. The best approach would be to parameterize all these structure domains per failure mechanism spatially and utilize them for the detailed quantitative rock slope susceptibility analysis.

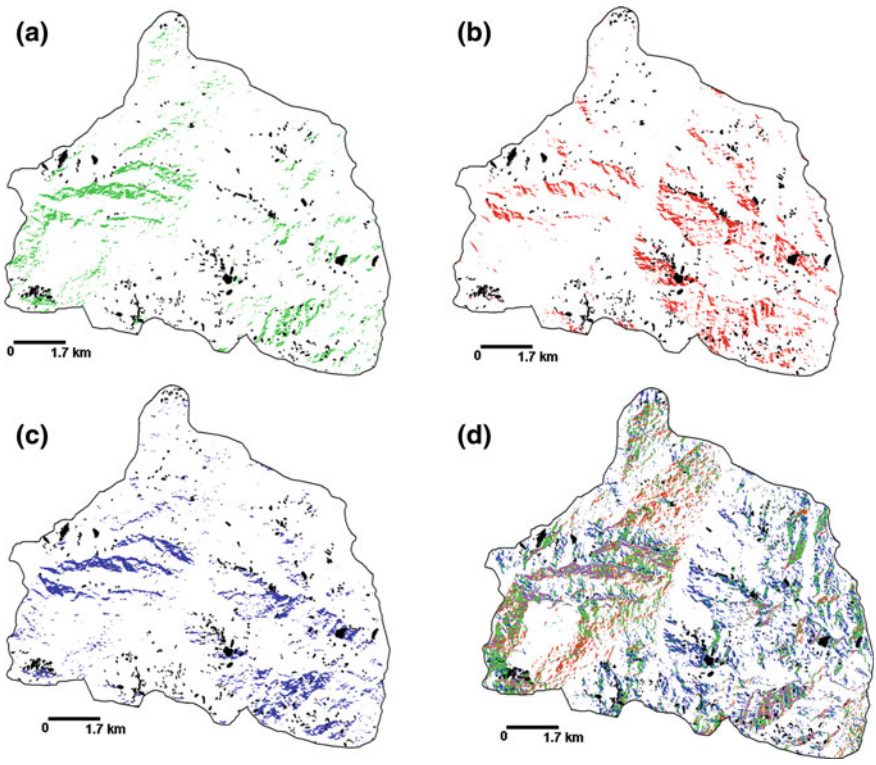


**Fig. 9.11** Preliminary results of the application of RSS-GIS in Kurseong area, Darjeeling district, India. **a** Planar failure modes caused by prominent foliation orientation. **b** Planar failure modes caused by one prominent joint plane. **c** Wedge failure modes caused by foliation and joint plane and **d** Combination of all failure modes (Black polygons are rock slides of 1968–2007)

### *9.4.3 Multivariate Statistical Analysis*

Landslide susceptibility can quantitatively be determined by a number of statistical and mathematical methods in a GIS using spatial relations of landslides and their relevant causal predictors. Amongst these, multivariate quantitative methods such as discriminant analysis (Carrara et al. 1991) and logistic regression (Mark and Ellen 1995) have proven to lead to better prediction results than other statistical methods, although the interpretation of the contribution of each causal parameter is less straightforward. Several multivariate susceptibility methods are available however there exists considerable difference between the scope of these methods and the usability of produced susceptibility maps (Aleotti and Chowdhury 1999; Brabb 1984; Chung and Fabbri 2008; Guzzetti et al. 1999; Soeters and van Westen 1996; van Westen et al. 1997). Thus, to ensure the quality of any quantitative prediction cross validation is necessary, which is best done by separating the

**Table 9.3** Contingency table (rock slides—discriminant analysis, 76.5% original grouped cases classified)

| Observed | | Non-landslide slope units | Landslide slope units | Total |
|---|---|---|---|---|
| Count | Non-landslide slope units | 667 | 188 | 855 |
| | Landslide slope units | 77 | 194 | 271 |
| % | Non-landslide slope units | 78.0 | 22.0 | 100 |
| | Landslide slope units | 28.4 | 71.6 | 100 |

landslide population into two independent groups—one for model calibration/training and the other for validation (Chung and Fabbri 1999, 2008; Chung 2003).

Multivariate statistical analysis of landslide susceptibility was carried out for the Kurseong area, where both logistic regression (LR) and discriminant analysis (DA) were applied. For this study, 342 shallow translational rock slides of pre-2004 period were used as the training data and 183 rock slides of 2004–2007 periods were used for cross-validation. Multivariate model calibration with such landslide data was carried out through establishing the multivariate spatial signature of different causal parameters/geofactors as relevant independent/explanatory/predictor variables in each terrain mapping unit against the presence or absence of calibrating landslides as grouping or dependent variables. In the study area, 1126 slope units were used as terrain mapping unit, which were semi-automatically derived through sub-division of the terrain into different small hydrological subunits. For this subdivision, digital topographic information from a 10 m × 10 m digital elevation model (DEM) was used along with ridge lines and drainages. This type of terrain sub-division has been successfully implemented by a number of authors in for predicting new landslides (Cardinali et al. 2002; Carrara 1999; Galli et al. 2008; Guzzetti et al. 2006; Van Den Eeckhaut et al. 2009).

Density of landslides in each of the slope units (1126) was calculated using the pre-2003 landslide inventory. The slope units (855) with landslide density >2% was considered as landslide prone and the rest (271) were grouped as landslide free. Nine relevant causal geofactor maps comprising different morphometric and geo-environmental parameters were used as explanatory variables. These include slope material, structure, geomorphology, land use, fracture density and aspect as categorical variables and minimum, maximum, range, mean and standard deviation of elevation, slope, rainfall, wetness index, curvature as continuous variables. The categorical explanatory variables were converted to their continuous equivalents by calculating the cumulative area percentage of each geofactor class for each mapping unit (slope unit).

The application of the DA and LR methods for rock slides resulted in an overall model classification of slope units (both landslide-bearing and non-landslide-bearing slope units) of 76.5% (Table 9.3) and 81.2% (Table 9.4) respectively with a receiver operator characteristic (ROC) area of 0.82 and 0.84 respectively. The resultant maps are shown in Fig. 9.12 and the ROC curves in Fig. 9.13. Both susceptibility maps shows moderate to high rate of *goodness-of-model-fit* and *prediction*, though, the performance of LR is comparatively better than the DA

**Table 9.4** Contingency table (rock slides—logistic regression, 81.2% original grouped cases classified)

| Observed | | Non-landslide slope units | Landslide slope units | Total |
|---|---|---|---|---|
| Count | Non-landslide slope units | 800 | 55 | 855 |
| | Landslide slope units | 157 | 114 | 271 |
| % | Non-landslide slope units | 93.6 | 6.4 | 100 |
| | Landslide slope units | 57.9 | 42.1 | 100 |

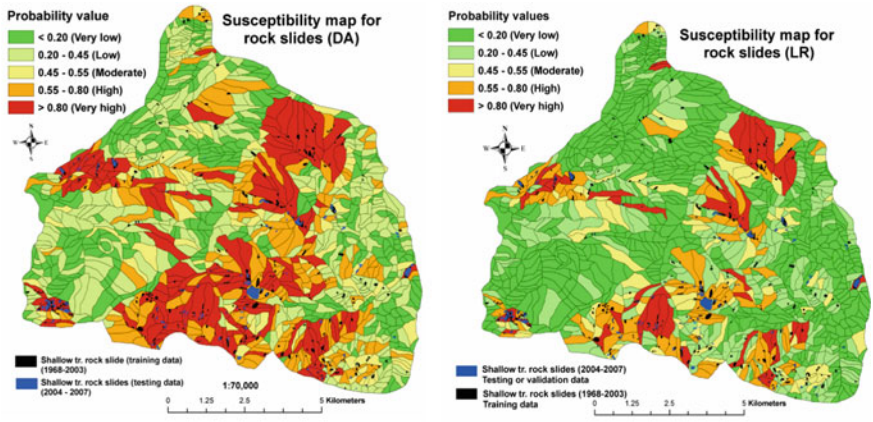


**Fig. 9.12** Susceptibility maps generated using Discriminant Analysis (*left*) and logistic regression (*right*)

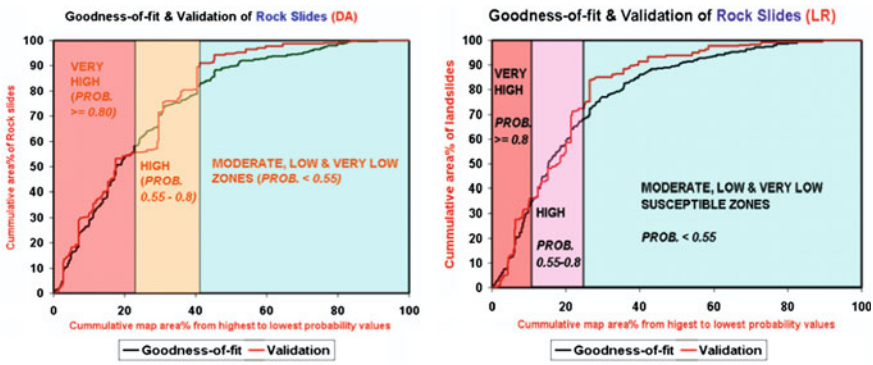


**Fig. 9.13** Success and prediction rate curves. *Left* Discriminant analysis. *Right* Logistic regression

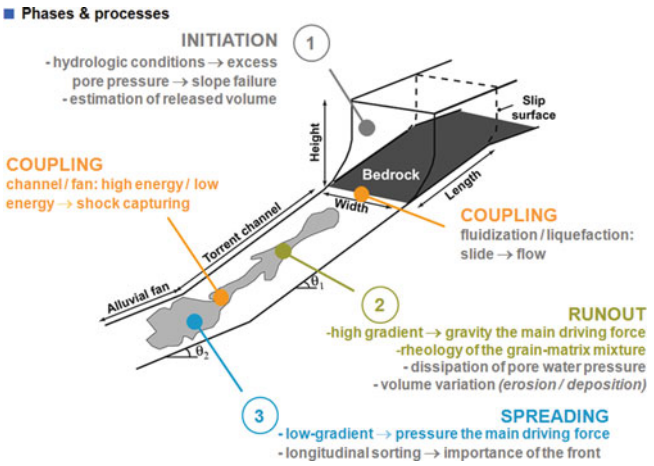


**Fig. 9.14** Chronological phases and processes in shallow landslides and consequent debris flows

model. With the DA model only 23% of the landslides in the validation data set could be explained, while using the LR 72–73% of the landslides in the validation data could be explained.

This research was a joint effort with researchers from IRPI, CNR, Italy. The multivariate statistical models used were either those readily available in SPSS 4.0® or R-scripts developed at IRPI CNR Perugia (IRPI CNR 2009). The preliminary results were presented by Ghosh et al. (2009b) in the European Geosciences Union General Assembly 2009.

### *9.4.4 Physical modeling of landslide initiation and runout*

Physically-based spatial modelling of landslide hazard necessitates the processes to be mathematically abstracted based on the known universal laws of physics (Davies 1992). The hazard area entails the three major chronological phases (Fig. 9.14): the initiation zone, transportation path and deposition fan (Chen and Lee 2004). Modelling this sequential chain of events by integrating the various governing equations into one model is complicated. This is due to the fact that the varying temporal and spatial scales of these processes will cause multi-dimensional uncertainties that cannot be quantitatively accounted. Hence, landslide initiation is modelled independent of landslide run-out; the run-out accounts for both transportation and deposition.

Physically-based models can be static or dynamic. Static models consider landslides in its stable state and seek to determine which stimuli caused the instability (Bromhead 1996). Dynamic models are capable to run forward in time, using rules of cause and effect to simulate temporal changes in the landscape

(Karssenberg 2002). A dynamic landslide hazard model addresses the spatial and temporal variation of landslide initiation (Brooks et al. 2004; van Beek and van Asch 2004) or runout (Cannon and Savage 1988; Rickenmann 2005). Even though physically-based models do not necessarily demand long term data, availability of such data can improve model calibration significantly. However, such models demand high spatial resolution and measurement precision for accurate predictions. With the increasing trend of quantitative studies in geomorphology, application of such models has substantial increased in the last two decades. Such models are valuable tools for quantitatively assessing the influence of various parameters contributing to the initiation (Kuriakose et al. 2009c) and runout of landslides.

### *9.4.5 The Models*

There are several physically-based spatial models capable of modelling the landslide initiation and runout, though attempts to adopt them to Indian conditions are limited. This article illustrates the application of a physically-based dynamic slope hydrology coupled slope stability model [STARWARS + PROBSTAB (Storage and Redistribution of Water on Agricultural and Re-vegetated Slopes + Probability of Stability) (van Beek 2002)] and a runout model [Mass-Mov 2D (Begueria et al. 2009)] in a landslide prone region in the Western Ghats of Kerala, India. STARWARS + PROBSTAB was developed by van Beek (2002). They comprise a distributed dynamic hydrological model (STARWARS) that is coupled to a stability model (PROBSTAB). The dynamic spatial outputs of the hydrological model are the inputs for the slope stability model. An added advantage of the models is that its open architecture allows modification of the model script and thereby enables different parameterizations appropriate for the study area. Both the models are embedded in PCRaster, a GIS with an advanced Environmental Modelling Language (www.pcraster.nl).

STARWARS was originally designed to evaluate the effects of vegetation on hillslope hydrology in SE Spain. Soil hydrological properties can be assigned to specific land use types and the model originally included the processes of interception and evapotranspiration. The amount of actual evapotranspiration is scaled to the available storage and FAO crop factors (Doorenbos and Pruitt 1977). It contains a detailed description of the unsaturated zone that is present in the soil mantle over a semi-impervious lithic contact, which in this case is the Charnockites. The soil profile is subdivided into three layers that can be interpreted as the A, B and C horizons. Percolation of soil moisture is driven by gravity and depends on the unsaturated hydraulic conductivity which is prescribed by the soil water retention curve of Farrel and Larson (1972) and the unsaturated hydraulic conductivity relationship of Millington and Quirk (1959). At the lower end of the soil mantle, the percolation into the underlying bedrock is impeded and a perched water table may form. The resulting perched water table will drain laterally according to the gradient of the phreatic surface. All

unsaturated fluxes are considered to be vertical only. PROBSTAB is based on the infinite slope model and as such is valid for translational slides (Skempton and DeLory 1957). This is consistent with the type of failures in the study area. PROBSTAB calculates Factor of Safety for the entire soil column (FOS), and if required the depth of failure ($Z_F$), based on the daily variation of water level and volumetric moisture content, which are the outputs of STARWARS. In addition, PROBSTAB uses the matric suction to calculate the unsaturated shear strength when a perched water table is absent using Fredlund's (1987) equation and it includes the mechanical effects of root reinforcement and surcharge on slope stability. Hence the calculated stability varies on a day-to-day basis with the hydrological input. The model is also capable of accounting for the probability of failure ($P_F$). Probability of failure was obtained using the first-order second moment (FOSM) approach (Ang and Tang 1984) which takes into account the uncertainty in the estimation of the mechanical effects of vegetation, shear strength parameters, soil depth and slope angle. FOSM method necessitates the assumption of a normal curve. The curve is implemented in the model with the first standard deviation on the positive and negative side for a given parameter. This draws from the assumption that by using the first standard deviation on either sides of the curve, 66.6% of the total possible variation of the parameter is captured. This is also a direct indicator of the sensitivity of the model to the parameter and thus can also partially address the issue of uncertainty in parameter estimation.

Owing to the data poor situation some modifications to the models and their dependency were made. For example, the model was modified to account for root-induced cohesion and surcharge that were not originally considered by van Beek (2002). Potential evapotranspiration (PET) was calculated outside the model environment using Hargreave's equation (Hargreaves and Samani 1982) which is less data demanding than the Penman's equation (Penman 1948) originally used by van Beek (2002). Interception was computed by means of "Aston's (1979)" equation (Eq. 1), and throughfall and evapotranspiration of the canopy storage was addressed outside the model environment. A detailed description of these modifications, calibration and application of the model in a larger area containing the study area can be found in Kuriakose et al. (2009c).

MassMov was developed by Begueria et al. (2009). It is linked to the PCRaster GIS package, and uses a fixed finite-differences mesh and a two-step Lax-type explicit numerical scheme with variable temporal resolution to ensure stability. The flow is modelled as a 2D continuum by using a depth-integrated form of the Navier–Stokes equations under the shallow water assumption (Saint–Venant equation). The flow behaviour is controlled by the resisting forces, for which a set of alternative rheological models can be used. For the present study Vollehmy rehology was chosen due to the known frictional behaviour of debris flows in the region. The model uses bed entrainment by defining an entrainment zone, a maximum depth of supply material and the average growth or erosion rate (McDougall and Hungr 2005).

**Table 9.5** Parameters used for simulating the debris flow using MassMov 2D (Voellmy Rheology)

| | |
|---|---|
| • Density of the DF: 2000 kg/m$^3$ | • DEM subtracted by soil depth (SD) at the initiation zone |
| • Chezy roughness: 250 m/s$^2$ | • Soil depth at the initiation zone: Initial volume—1669 m$^3$, Initiation area—782 m$^2$, Area affected by scouring—2337 m$^2$ |
| • Angle of basal friction: 30° | • Soil depth along the runout and deposition zones |
| • Angle of internal friction: 35° | |
| • Density of the soil: 2000 kg/m$^3$ | |
| • Scouring rate: 0.0035 m/s | |
| • Fluid rate: 10 m/s (Transition from solid to fluid) | |
| • Total time steps: 100 s | |

### *9.4.6 The Data*

The models were tested in the study area in Kerala (Fig. 9.2). The slope hydrology coupled slope stability model was applied in Aruvikkal catchment, a 9.5 km$^2$ sub-catchment of Tikoy River which in turn is a tributary of the Meenachil River. The run-out was tested on a specific landslide that occurred near Peringalam village in the upper reaches of Meenachil River. All necessary data for STARWARS + PROBSTAB were derived from preceding research works and associated field work (Kuriakose et al. 2009a; Thampi et al. 1998). The data available were daily rainfall, crop factors, potential evapotranspiration, MODIS NDVI 16 day composites, soil types, soil properties, contour map from topographic sheet, soil depth, root cohesion, soil depth, root cohesion, land use/land cover and a rudimentary landslide inventory containing only the date and the location of events. Calibration and validation was also carried out in a similar manner as described in Kuriakose et al. (2009a). The model validation was carried out for the year 2001 as the study area experienced six shallow landslides on 8th July 2001. The DEM and other spatially parameterized data had a spatial resolution of 10 m by 10 m.

Data such as the deposit area and depth of the Peringalam landslide necessary for calibrating and validating MassMov2D was generated during a field survey in 2007 using simple hand held Garmin GPS and information of final deposit height collected by interviews with the local inhabitants. Initial volume and scouring data was also generated in a similar manner. The pre event DEM with 1 m resolution of the area was derived from a 20 m interval contour map of the region prepared based on a survey conducted in the 1970s and interpolating the field survey points that were outside the landslide body. The parameters and the calibrated values of each of them as used in MassMov2D are provided in Table 9.5. The model was

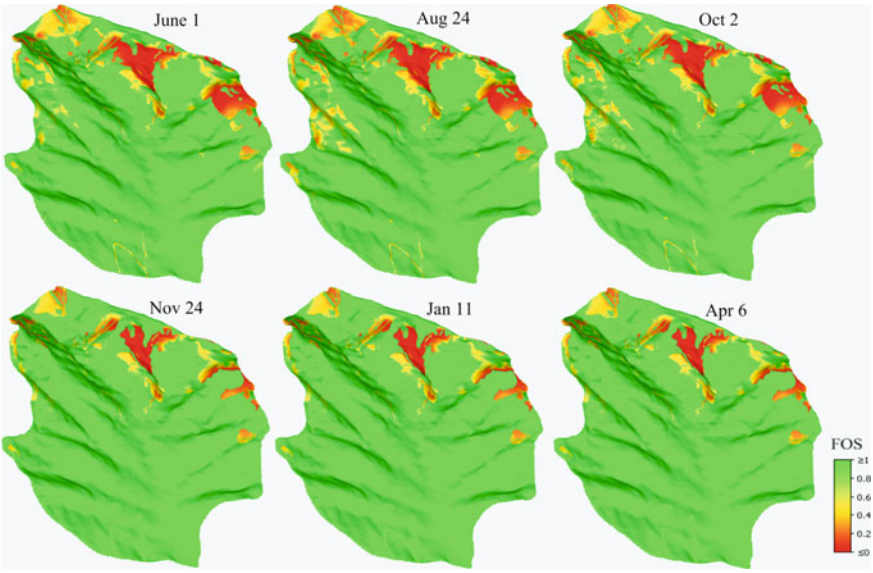


**Fig. 9.15** Daily variation of factor of safety in the year 2001—Predicted by STARWARS + PROBSTAB

calibrated based on the volume of deposit and was cross validated with the observed area and depth of failure.

### *9.4.7 The Results*

The model simulated transient hydrological and slope stability conditions on a daily time step with (Fig. 9.15) and without considering vegetation effects. A detailed investigation revealed that the hydrological effects of vegetation are crucial for the long term stability of the study area. However, its effects on slope stability during high intensity rainfall are negligible. Mechanical effect of vegetation, especially root induced cohesion was the most significant effect of vegetation on slope stability in the region. The unstable area (FOS <1) as calculated by the model, considering vegetation effects was 2.1 $km^2$ (Fig. 9.16a); without considering vegetation effects the unstable area was 5.5 $km^2$ (Fig. 9.16b). About 0.8 $km^2$ of this area was persistently unstable (FOS <1) which may be attributed to the inaccurate parameterization in such areas. This over estimation of unstable area was in agreement with similar studies elsewhere (Simoni et al. 2008; van Beek and van Asch 2004). Sensitivity analysis indicated that the FOS was the most sensitive to slope, angle of internal friction and soil depth (Fig. 9.17). The DEM resolution of 10 m derived from a 20 m contour map interpolation was also a significant contributor to the overestimation. All six landslide locations were predicted as failed on

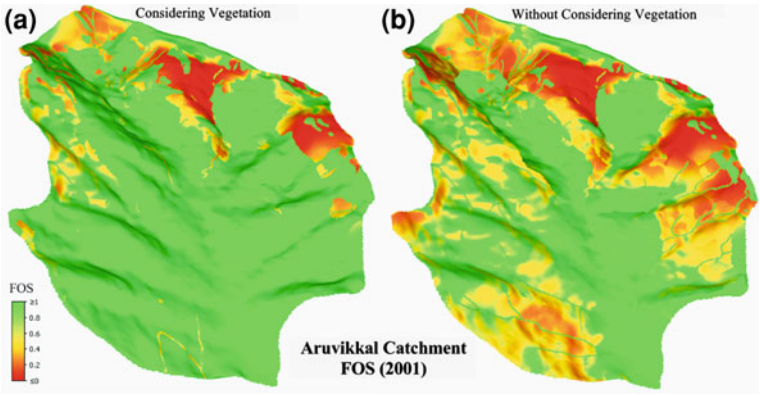


**Fig. 9.16** Minimum factor of safety of every pixel (2001). **a** Considering vegetation and **b** Without considering vegetation

**Fig. 9.17** Sensitivity of PROBSTAB to parameters

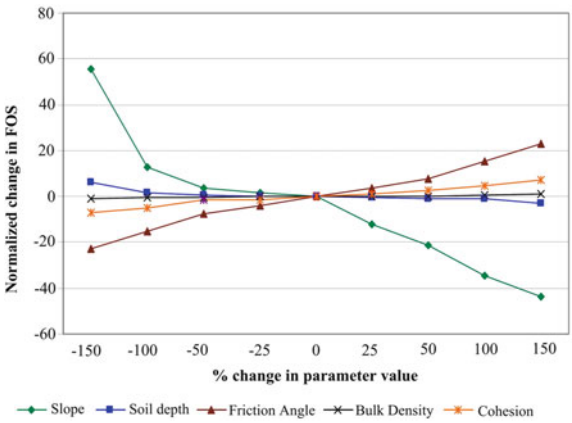


the known date of failure with $P_F$ (FOS <1) $\geq$ 60% indicating accurate temporal predictive capability of the model.

The slope-stability modelling indicates that the antecedent moisture conditions and the persistence of high pore-water pressure for a significantly long period may have been the immediate preparatory conditions for the failures. The trigger of the events was probably an extremely high intensity rainfall which resulted in a sharp increase of pore-water pressure. This response pattern was also apparent from the instrumented monitoring of hollows in the region (Kuriakose et al. 2008). The research conclusively highlights the significance of vegetation effects on slope stability. Better input data, especially DEM and soil depth can significantly improve the predictions.

Table 9.6 shows the comparison of predicted to observed properties of the debris flow. Figure 9.18 shows the temporal evolution of the debris flow height as

**Table 9.6** Comparison of observed and predicted properties of the debris flow

| | Observed | Predicted by MassMov 2D |
|---|---|---|
| Initial volume ($m^3$) | 443 | |
| Entrained volume ($m^3$) | 1226 | 813 |
| Total volume ($m^3$) | 1669 | – |
| Total deposit volume ($m^3$) | 1553 | 1253 |
| Max. velocity (m/s) | 1.5 min to reach 180 m | 24 |
| Mean max. velocity (m/s) | | 21 |
| Min. deposit thickness (m) | 0.1 | 0.1 |
| Mean deposit thickness (m) | 1.2 | 1.7 |
| Max. deposit thickness (m) | 6.4 | 3.5 |
| Deposit area ($m^2$) | 2686 | 1634 |
| Observed deposit area overlaid by predicted deposit area (%) | | 61 |

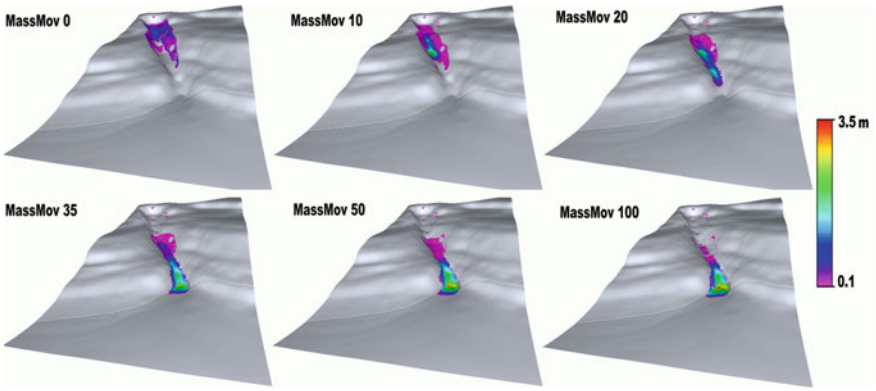


**Fig. 9.18** Temporal evolution of debris flow height as predicted by MassMov2D

predicted by the model. The predicted deposit volume was underestimated; the discrepancy was not of very high orders. It has to be noted that the field survey of the slide occurred after three years causing errors in the estimation of the slide body and volume. A part of the material (the slurry) may have been eroded over time resulting in the underestimation of the observed deposit volume. The predicted deposit area was grossly underestimated. This can be attributed to the fact that in reality, the moving mass is not uniform in its rehology.

Improving the run-out model predictions necessitate high resolution DEM (>1 m). Methods for incorporating the transient rheology of the flow should be attempted. Immediate surveys after the occurrence of the events is a necessity such that accurate estimates of initial volume, scoured volume and deposit volume can be made.

The present study was an attempt to evaluate the hazard quantification potential of physically based models in data poor regions. Although both STARWARS + PROBSTAB and MassMov provided outputs that have physical meaning it was

not possible to conduct an appropriate evaluation of the model performance due to the limited nature of the calibration and validation data. Thus the results are merely indicative of what can be achieved by using such models for a quantitative evaluation of landslide hazard.

It is evident from this study that physically-based spatial models are ideal to quantitatively understand the contribution of a specific parameter towards landslide hazard. As need is a motive for quality, it is certain that with more and more researchers turning their attention towards utilizing physically-based models, data quality will improve over time.

## 9.5 Risk Assessment

The landslide risk definition given by Varnes and IAEG Commission on Landslides and other Mass-Movements (1984) can be represented by the following equation (van Westen et al. 2006):

$$Risk = \sum \left( H \sum (VA) \right) \tag{2}$$

$$R_{prop} = \left\{ \sum_{i=1}^{k} \left[ H_i x P_{T:L} x P_{S:T} x V_{prop:i} \right] x A \right\} \tag{3}$$

where, $R_{prop}$ is the expected loss to the infrastructure property due to landsliding in a given return period, $H_i$ is the hazard due to a landslide with a magnitude '*i*' in a given return period, $P_{T:L}$ is the probability of a landslide with a magnitude '*i*' reaching the infrastructure, $P_{S:T}$ is the temporal spatial probability of the infrastructure, $V_{prop:i}$ is the vulnerability of the infrastructure property for a landslide of magnitude '*i*', and $A$ is the cost of making one kilometer of a new infrastructure. The landslide belongs to different magnitude class ranging from I to IV. The specific risk for the two important infrastructure properties i.e. the railroad (*Rs_rl*) and the highway road (*Rs_rd*) can be estimated by using Eq (3). The value of $P_{S:T}$ is taken as 1.0 as both the elements are stationary object and always remain on or in the path of the landslide. The value of $P_{T:L}$ is also taken as 1.0 as the hazard was estimated for landslides that affect the infrastructures. The assessment of vulnerability can be based on the detailed analysis of the past damage records. The degree of damage can be either monetary or physical (structural damage).

The study are in Nilgiri with the railroad and road was selected as study site for the risk assessment, as it has detailed landslide data as well as traffic information. The infrastructure vulnerability was calculated as the ratio of the total restoration cost of the damaged infrastructure due to a landslide of a given type and magnitude to the actual cost of constructing one kilometer of new railroad or tarmaced road. The total restoration cost of the railroad includes cost of removing debris of magnitude '*i*' and cost of replacing the damaged rail structure (i.e. rail, rake bar, sleeper and pebbles). Vulnerability in terms of the physical loss to the railroad and

**Table 9.7** Vulnerability for elements at risk when hit by a landslide

| Type of element at risk | Vulnerability in different magnitude class | | | | Comments |
|---|---|---|---|---|---|
| | I | II | III | IV | |
| Physical damage to a infrastructure | | | | | Damaged caused by one landslide of a given magnitude in one kilometer |
| Railroad | 0.01 | 0.08 | 0.25 | 0.60 | |
| Road (Asphalt) | 0.001 | 0.01 | 0.10 | 0.50 | |
| Physical damage to a moving vehicle | | | | | Damaged calculated based on past records |
| Bus | 0.01 | 0.10 | 0.80 | 1.0 | |
| Lorry | 0.01 | 0.10 | 0.80 | 1.0 | |
| Car | 0.10 | 0.50 | 1.0 | 1.0 | |
| Motorbike | 0.50 | 0.80 | 1.0 | 1.0 | |
| Person in a moving vehicle | | | | | Damaged calculation partly based on past incidents and expert judgment |
| Bus | 0.001 | 0.10 | 0.80 | 1.0 | |
| Lorry | 0.001 | 0.10 | 0.80 | 1.0 | |
| Car | 0.01 | 0.10 | 1.0 | 1.0 | |
| Motorbike | 0.50 | 1.0 | 1.0 | 1.0 | |

the road due to a landslide of magnitude I, II, III and IV is given in Table 9.7. Maximum vulnerability for the railroad (0.6) and for the road (0.5) was obtained for landslide of magnitude IV and the value decreases with the decrease in the size of the landslide.

The risk to a moving vehicle, i.e. a vehicle being hit by a landslide, largely depends on the temporal spatial probability of the vehicle at the time of occurrence of the landslide. This value of probability ($P_{S:T}$) can be used to calculate risk to a moving vehicle by using the following three expressions (AGS 2000):

$$R_v = \left\{ \sum_{i=1}^{k} \left[ P(V) x V_{veh:j} x N_v \right] \right\} \tag{4}$$

$$P(V_i) = 1 - \left(1 - (P_{S:T})^{NR}\right) \tag{5}$$

$$P_{S:T} = (ADT\, x\, L\, x\, SL)/(24\, x\, 1000\, x\, V_v) \tag{6}$$

where, $R_v$ is the expected loss of vehicles of a given type due to landsliding in a given return period ($), $P(V_i)$ is the probability of the vehicle being hit by a landslide with a magnitude '$i$', $V_{veh:i}$ is the vulnerability of the vehicle for a landslide of magnitude '$i$', $A$ is the cost of the vehicle ($), $N_v$ is the number of vehicles of a given type in a landslide zone at any given time, $P_{S:T}$ is the temporal spatial probability of the vehicle, $NR$ is the number of landslides of magnitude '$i$' reaching the transportation line in a given return period, $ADT$ is the average daily traffic (vehicles per day), $L$ is the average length of the vehicle (m), $SL$ is the length of the landslide affected zone (km), and $V_v$ is the velocity of the vehicle (km/hr).

In this chapter, the assessment of vulnerability of different types of moving vehicles (bus, lorry, car and motorbike) and train for a landslide of magnitude '*i*' is carried out based on the historical records, experience of the local people and expert knowledge. Other variables were obtained from historical records and field calculations. The average speed for the road cruising vehicles and train was measured as 26 and 11 km/hr, respectively. The ADT for bus, lorry, car and motorbike was obtained as 137, 309, 554 and 90 vehicles per day, respectively and for train it is two per day. The length of landslide affected zone (*SL*) along the road and the railroad was calculated from landslide density, which is the ratio of the total landslide scar width to the total length of the transportation line. The total *SL* along the road and the railroad is 2.1 and 3.84 km, respectively. The average length (*L*) of a bus, lorry, car, motorbike and train was measured as 12, 8, 5, 2 and 55 m, respectively. By using the above values and Eqs (4–6) specific risk to a bus (Rs_b), lorry (Rs_l), car (Rs_c), motorbike (Rs_mb) and train (Rs_t) in terms of monetary loss ($) can be calculated for each hazard scenario.

The risk of life or the annual probability of a person losing his/her life while travelling in a vehicle depends on the probability of the vehicle being hit by a landslide and the probability of death of the person (vulnerability) given the landslide impact on the vehicle. The vulnerability of commuter to a landslide depends on the type, speed and size of the landslide, the speed and type of the vehicle, and whether the person is in the open or enclosed in a vehicle (Wilson et al. 2005). It also depends on whether the debris have directly hit the vehicle from the top or moved horizontally and hit the side of the vehicle. Even with the availability of some known incidents and damaged records the assessment of vulnerability of death still remains fuzzy. Due to such large variability of factors the assessment of vulnerability was somewhat subjective and knowledge driven. The risk of life for the commuters travelling along the road using different mode of travel such as bus, lorry, car or motorbike, and also in the train were estimated. The analysis shows that the annual probability of the person most at risk losing his/her life by driving along the road in a hazard of 3, 5, 15, 25 and 50 years return period is $1.3 \times 10^{-6}$, $2.6 \times 10^{-6}$, $5.2 \times 10^{-6}$, $6.3 \times 10^{-6}$ and $7.8 \times 10^{-6}$ persons/annum, respectively. Along the railroad these values are $6.8 \times 10^{-3}$, $1.0 \times 10^{-2}$, $1.7 \times 10^{-2}$, $2.0 \times 10^{-2}$, $2.4 \times 10^{-2}$ persons/annum, respectively.

The total landslide risk is the summation of all the specific risks related to landslides in an area. In this study, total landslide risk in terms of the monetary loss was calculated by adding all the specific direct and indirect risks evaluated for 24 hazard scenarios as described above:

$$\begin{aligned} RT(P) &= \sum_{h=1}^{24} [RD + RI] \\ &= \sum_{h=1}^{24} [(RS\_rl + RS\_rd + RS\_b + RS\_l + RS\_c + RS\_mb + RS\_t) + RI] \end{aligned} \tag{7}$$

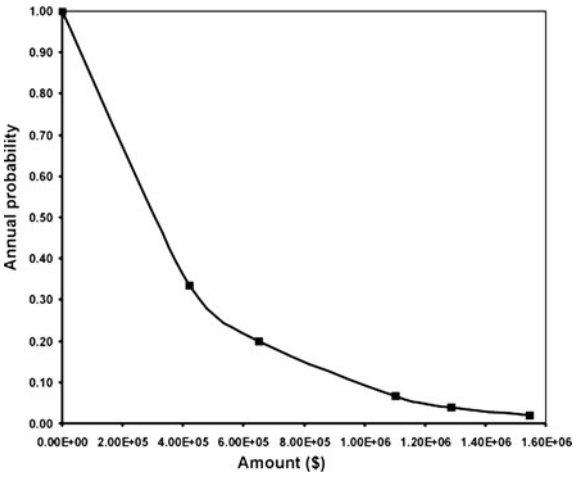


**Fig. 9.19** Curve including both direct and indirect losses expressed in monetary value (in US $)

where, *RT(P)* is total risk for monetary loss expressed in US dollars. The total landslide risk for the loss of life, *RT(D)* expressed as number of people per annum was calculated by adding all specific loss of lives such as:

$$RT(D) = \sum_{h=1}^{24} [RS\_Db + RS\_Dl + RS\_Dc + RS\_Dmb + RS\_Dt] \qquad (8)$$

.

The occurrence of a certain number of landslides will incur indirect loss resulting from the temporary interruption of the road (NH67) and the railroad. The indirect loss for additional fuel consumption due to the detour was calculated. The total loss for the 24 hazard scenarios amounts to $ 963470 of which the loss to Nilgiri and tourists vehicles was $ 790570 and $ 172900, respectively. In the event of the interruption of NH67 the daily commuters have to travel an additional 32 km for which they have to bear additional tickets cost for a longer journey.

Besides commuters the traffic interruption also affects the local business along NH67 and their livelihood which is totally dependent on tourists travelling along the road. The indirect loss of income for business around Katteri and Burliyar area was estimated. The total loss for the 24 hazard scenarios amounts to $ 912, $ 3009, $ 27512 for shops, commodity and liquor business respectively, located in Katteri and $ 10640 for shops in Burliyar. Besides national highway, the railroad is also prone to interruption due to landslides. The revenue loss to the railway company was estimated for all hazard scenarios, for a 50 years return period. The blockage period for the railroad is much higher than the road for a given landslide. The cumulative loss from the 24 hazard scenarios was $ 677419.

The total indirect loss resulting from the traffic interruption of the road and the railroad by landslides in six return periods amounts to $ 1801525, and in 3, 5, 15, 25, and 50 years return period it was estimated to be around $ 147580, $ 233921, $

398,283, $ 464982 and $ 556758, respectively. The total direct loss for all the hazard scenarios amounts to $ 3205711 and in 3, 5, 15, 25, and 50 years return period it was estimated to be around $ 273756, $ 416611, $ 703160, $ 822896 and $ 989286, respectively. The total risk for all hazard scenarios was estimated as $ 5007236. Similarly, human fatalities as a consequence of vehicles and trains being directly hit by landslides were estimated to be 15 persons per year. The output of the result is displayed as a risk curve, containing the relation between hazard with different annual probabilities and the corresponding total specific losses (Fig. 9.19). The result indicates that the loss.

## 9.6 Conclusions

Risk assessment is the final step in a chain of scientific and methodological preludes for disaster risk reduction. Thus uncertainties from all the previous steps propagate to this logical culmination of landslide hazard and risk analysis. Despite the explicit uncertainties in quantifying risk and defining vulnerability, landslide risk assessment is a formal land use planning necessity in several developed countries, especially along transportation lines. In India, Several human fatalities are reported annually as a direct consequence of landslides in the country. The sectors that are affected by continuous landslide problems are fairly well known and thus the need of the hour is to develop pragmatic remedial measures such as bio-engineering methods and structural designs capable of reducing slope instability conditions.

In January 2009 a panel discussion was held at the head office of the Geological Survey of India on some of the problems and possible solutions for a uniform and relevant method of medium-scale landslide hazard and risk assessment in India. Some of the conclusions were that:

- India should consider conducting landslide susceptibility mapping as the first step towards a comprehensive landslide hazard and risk assessment and follow this up with detailed analysis for specific areas.
- It is doubtful whether a uniform methodology can be applied to all landslide prone regions of India given the varied geological and climatic conditions. Hence, generalized susceptibility mapping approaches applicable for different landslide prone regions of the country are to be developed taking into account this variability in the prevailing environmental conditions. Also specific methods for different landslide types are required.
- Attention should on maintaining the uniformity of the output maps, which is extremely important for proper understanding by planners and other end user agencies. The scale of mapping for regional assessment could be 1:50,000. The output map may depict only three classes of susceptibility, “Low” containing $<2\%$ of all landslides, “Moderate” having $\pm 8\%$ of all landslides and “High” $>90\%$ of all landslides.

- The existing BIS guidelines completely ignores the necessity of a detailed landslide inventory, which is an extremely important input for a comprehensive hazard and risk assessment. A team of dedicated and trained experts should be employed to generate such a detailed landslide inventory using aerial photographs, stereo image interpretation and other ancillary datasets. Subsequently, a heuristic approach using a weighting system of geofactors may be adopted that is relevant to specific geo-environments (taking into account the landslide inventory), which could then be used to generate the susceptibility map. Statistical methods or Spatial Multi Criteria Evaluation (SMCE) could be an alternative to the heuristic weighting and rating method, depending on the availability of data and the choice of the researcher.
- The methods should be reproducible and scientifically dependable and clearly specify how the maps have been prepared and validated. For validation, the importance of using independent landslide inventory data is recommended.

GSI should work in tandem with other similar organizations in India to develop an open-source, web-based *National Landslide Database* containing information about landslide type, dimension, location, time of occurrence, topographic characteristics, etc. Though this may seem to be an enormous undertaking, given the state-of-the-art communication network and the participation and sharing of data between large numbers of interested working groups in central and state level organizations/institutions, it is quite feasible in India. It is reiterated here that an up-to-date landslide inventory is absolutely essential, without which a comprehensive landslide hazard and risk analysis is impossible.

## References

AGS (2000) Landslide risk management concepts and guidelines (Prepared by Australian Geomechanics Society, Sub-committee on Landslide Risk Management). Aust Geomech 35(1):49–92

Aleotti P, Chowdhury R (1999) Landslide hazard assessment: summary review and new perspectives. Bull Eng Geol Environ 58(1):21–44

Anbalagan R (1992) Landslide hazard evaluation and zonation mapping in mountainous terrain. Eng Geol 32(4):269–277

Anbalagan R, Singh B (1996) Landslide hazard and risk assessment mapping of mountainous terrains—a case study from Kumaun Himalaya India. Eng Geol 43(4):237–246

Ang AH-S, Tang WH (1984) Probability concepts in engineering planning and design: decision, risk, and reliability (V II). Wiley, New York, 562 pp

Aston AR (1979) Rainfall interception by eight small trees. J Hydrol 42(3–4):383–396

Barlow J, Martin Y, Franklin SE (2003) Detecting translational landslide scars using segmentation of Landsat ETM + and DEM data in the northern Cascade Mountains, British Columbia. Can J Remote Sens 29(4):510–517

Basu SR, De SK (2003) Causes and consequences of landslides in Darjeeling-Sikkim Himalayas. Geogr Polonica 76(2):37–52

Begueria S, van Asch TWJ, Malet J-P, Gröndahl S (2009) A numerical simulation model of the propagation and deposition of mud and debris flows over complex terrain—Model description

and modes of use. URL: http://digital.csic.es/handle/10261/11804?idioma=en. Accessed 15 May 2009
Bhattacharya A, Mishra P, Ghoshal TB, Bahuguna H, Ghatak T (1998) A geotechnical appraisal of landslides on 7th July, 1998 along National Highway No. 55, Progress report. Geological Survey of India, Government of India
BIS (1998) Preparation of landslide hazard zonation maps in mountainous terrains, IS 14496 (Part-2)— Guidelines. Bureau of Indian Standards Government of India, New Delhi
Blaschke T, Strobl T (2001) What's wrong with pixels? some recent developments interfacing remote sensing and GIS. GeoBIT/GIS, pp 12–17
Brabb E (1984) Innovative approaches to landslide hazard mapping. In:Proceeding of the IVth international symposium on landslides, Toronto, pp 307–324
Briggs RP (1974) Overdip slopes that can affect landsliding in Allegheny County, Pennsylvania. U.S. Geological Survey, Misc. Field Studies Map, MF-543
Bromhead E (1996) Slope stability modeling: an overview. In: Dikau R, Brunsden D, Schrott L, Ibsen M (eds) Landslide recognition: identification, movement and causes. Wiley, Chichester, pp 231–235
Brooks SM, Crozier MJ, Glade TW, Anderson MG (2004) Towards establishing climatic thresholds for slope instability: use of a physically-based combined soil hydrology-slope stability model. Pure Appl Geophys 161(4):881–905
Cannon SH, Savage WZ (1988) A mass change model for the estimation of debris flow runout. J Geol 96:221–227
Cardinali M, Reichenbach P, Guzzetti F, Ardizzone F, Antonini G, Galli M, Cacciano M, Castellani M (2002) A geomorphological approach to the estimation of landslide hazards and risks in Umbria, Central Italy. Nat Hazards Earth Syst Sci 2(1–2):57–72
Carrara A (1993) Potentials and pitfalls of GIS technology in assessing natural hazards. In: Guzzetti F, Reichenbach P, Carrara A (eds) Geographical information systems in assessing Natural Hazards—Abstracts. CNR, Perugia, pp 128–137
Carrara A (1999) Use of GIS technology in the prediction and monitoring of landslide hazard. Nat Hazards 20(2):117–135
Carrara A, Cardinali M, Detti R, Guzzetti F, Pasqui V, Reichenbach P (1991) GIS techniques and statistical models in evaluating landslide hazard. Earth Surf Proc Landf 16(5):427–445
Carro M, De Amicis M, Luzi L, Marzorati S (2003) The application of predictive modeling techniques to landslides induced by earthquakes: the case study of the 26 September 1997 Umbria-Marche earthquake (Italy). Eng Geol 69(1–2):139–159
Catani F, Casagli N, Ermini L, Righini G, Menduni G (2005) Landslide hazard and risk mapping at catchment scale in the Arno river basin. Landslides 2(4):329–342
Chen H, Lee CF (2004) Geohazards of slope mass movement and its prevention in Hong Kong. Eng Geol 76(1–2):3–25
Chung C-JF (2003) Validation of spatial prediction models for landslide hazard mapping. Nat Hazards 30(3):451–472
Chung CJF, Fabbri AG (1999) Probabilistic prediction models for landslide hazard mapping. Photogramm Eng Remote Sens 65(12):1389–1399
Chung C-J, Fabbri AG (2008) Predicting landslides for risk analysis—spatial models tested by a cross-validation technique. Geomorphology 94(3–4):438–452
Coe JA, Michael JA, Crovelli RA, Savage WZ, Laprade WT, Nashem WD (2004) Probabilistic assessment of precipitation-triggered landslides using historical records of landslide occurrence, Seattle, Washington. Environ Eng Geosci 10(2):103–122
Cruden D, Varnes DJ (1996) Landslide types and processes. In: Turner AK, Schuster RL (eds) Landslide: investigations and mitigation. special report 247. Transportation research Board. National Research Council. National Academy Press, Washington, pp 36–75
Davies P (1992) The mind of God—the scientific basis for a rational world. Simon & Schuster Inc, London, 256 pp

De Kok R, Schneider T, Ammer U (1999) Object based classification and applications in the Alpine forest environment fusion of sensor data knowledge sources and algorithms. ISPRS/EARSeL Workshop, Valladolid

Doorenbos J, Pruitt WO (1977) Crop water requirements. Irrigation and drainage paper 24. Food and Agriculture Organization of the United Nations, Rome

Farrel D, Larson W (1972) Modelling the pore structure of porous media. Water Resour Res 8:699–705

Fell R, Corominas J, Bonnard C, Cascini L, Leroi E, Savage WZ, Joint Technical Committee on Landslides and Engineered Slopes (JTC-1) (2008) Guidelines for landslide susceptibility, hazard and risk zoning for land use planning. Eng Geol 102(3–4):85–98

Fell R, Ho KKS, Lacasse S, Leroi E (2005) A framework for landslide risk assessment and management. In: International conference on landslide risk management, Vancouver, May 31–Jun 3 2005

Flanders D, Hall-Bayer M, Pereverzoff J (2003) Preliminary evaluation of eCognition object-based software for cut block delineation and feature extraction. Can J Remote Sens 29(4):441–452

Fredlund DG (1987) Slope stability analysis incorporating the effect of soil suction. In: Anderson MG, Richards KS (eds) Slope stability: geotechnical engineering and geomorphology. Wiley, Chichester, pp 113–144

Galli M, Ardizzone F, Cardinali M, Guzzetti F, Reichenbach P (2008) Comparing landslide inventory maps. Geomorphology 94(3–4):268–289

Ghosh S, van Westen CJ, Carranza EJM, Jetten VG (2009a) Generation of event-based landslide inventory maps in a data-scarce environment: case study around Kurseong, Darjeeling district, West Bengal, India. In: Malet JP, Bogaard TA, van Beek LPH, de Jong SM, Remaitre A (eds) Landslide processes: from geomorphologic mapping to dynamic modelling—A tribute to Prof Dr. Theo van Asch. CERG and Utrecht University, Strasbourg

Ghosh S, Reichenbach P, Rossi M, Guzzetti F, Cardinali M, van Westen CJ, Carranza EJM, (2009b) Influence of landslide types for calibrating different multivariate landslide susceptibility models. European Geosciences Union Annual General Assembly 2009, Vienna, Geophysical Research Abstracts Vol 11(EGU2009-13564), URL: http://meetingorganizer.copernicus.org/EGU2009/EGU2009-13564.pdf

Giles PT, Franklin SE (1998) An automated approach to the classification of the slope units using digital data. Geomorphology 21(3–4):251–264

Gumbel EJ (1958) Statistics of extremes. Columbia University Press, New York, 375 pp

Günther A (2005) RSS-GIS GridMap-Extension. Federal institute for geosciences and natural resources, Hannover. URL: http://www-public.tu-bs.de:8080/~aguenthe/rss-gis/. Accessed 10 May 2009

Günther A, Carstensen A, Pohl W (2004) Automated sliding susceptibility mapping of rock slopes. Nat Hazards Earth Syst Sci 4(1):95–102

Guthrie RH, Evans SG (2004) Magnitude and frequency of landslides triggered by a storm event, loughborough inlet, British Columbia. Nat Hazards Earth Syst Sci 4(3):475–483

Guzzetti F, Carrara A, Cardinali M, Reichenbach P (1999) Landslide hazard evaluation: a review of current techniques and their application in a multi-scale study central Italy. Geomorphology 31(1–4):181–216

Guzzetti F, Cardinali M, Reichenbach P, Carrara A (2000) Comparing landslide maps: a case study in the upper Tiber River Basin, central Italy. Environ Manage 25(3):247–263

Guzzetti F, Malamud BD, Turcotte DL, Reichenbach P (2002) Power-law correlations of landslide areas in central Italy. Earth Planet Sci Lett 195(3–4):169–183

Guzzetti F, Cardinali M, Reichenbach P, Cipolla F, Sebastiani C, Galli M, Salvati P (2004) Landslides triggered by the 23 November 2000 rainfall event in the Imperia Province, Western Liguria Italy. Eng Geol 73(3–4):229–245

Guzzetti F, Reichenbach P, Cardinali M, Galli M, Ardizzone F (2005) Probabilistic landslide hazard assessment at the basin scale. Geomorphology 72(1–4):272–299

Guzzetti F, Reichenbach P, Ardizzone F, Cardinali M, Galli M (2006) Estimating the quality of landslide susceptibility models. Geomorphology 81(1–2):166–184
Hansen A (1984) Landslide hazard analysis. In: Brunsden D, Prior E (eds) Slope instability. Wiley, New York, pp 523–602
Hargreaves GH, Samani ZA (1982) Estimating potential evapotranspiration. J Irrigation Drainage Eng, 108(IR3):223–230
Harp EL, Jibson RL (1996) Landslides triggered by the 1994 Northridge, California earthquake. Seismological Soc Am Bull 86:S319–S332
Hocking G (1976) A method for distinguishing between single and double plane sliding tetrahedral wedges. Int J Rock Mech Min Sci 13(7):225–226
Hoek E, Bray JW (1981) Rock slope engineering. Institute of Mining and Metallurgy, London 358 pp
IRPI CNR (2009) Tools—various software tools prepared or used by members of our team, or by scientists working with IRPI CNR. Instituto di Ricerca per la Protezione Idrogeologica, Perugia, Italy. URL: http://geomorphology.irpi.cnr.it/tools. Accessed 10 May 2009
Jaiswal P, van Westen CJ (2009) Estimating temporal probability for landslide initiation along transportation routes based on rainfall thresholds. Geomorphology. doi:10.1016/j.geomorph.2009.05.008
Karssenberg D (2002) Building dynamic spatial environmental models. PhD Thesis, University of Utrecht, The Netherlands, 222 pp
Kuriakose SL, Jetten VG, van Westen CJ, Sankar G, van Beek LPH (2008) Pore water pressure as a trigger of shallow landslides in the Western Ghats of Kerala, India: some preliminary observations from an experimental catchment. Phys Geogr 29(4):374–386
Kuriakose SL, van Beek LPH, van Westen CJ (2009a) Parameterizing a physically based shallow landslide model in a data poor region. Earth Surf Proc Land 34(6):867–881
Kuriakose SL, Sankar G, Muraleedharan C (2009b) History of landslide susceptibility and a chorology of landslide prone areas in the Western Ghats of Kerala. India Environ Geol 57(7):1153–1568
Kuriakose SL, Devkota S, Rossiter DG, Jetten VG (2009c) Prediction of soil depth using environmental variables in an anthropogenic landscape, a case study in the Western Ghats of Kerala. India Catena. doi:10.1016/j.catena.2009.05.005
Lu D, Mausel P, Brondizio E, Moran E (2004) Change detection techniques. Int J Remote Sens 25(12):2365–2407
Malamud BD, Turcotte DL, Guzzetti F, Reichenbach P (2004) Landslide inventories and their statistical properties. Earth Surf Proc Land 29(6):687–711
Mantovani F, Soeters R, van Westen CJ (1996) Remote sensing techniques for landslide studies and hazard zonation in Europe. Geomorphology 15(3–4):213–225
Mark RK, Ellen SD (1995) Statistical and simulation models for mapping debris-flow hazard. In: Carrara A, Guzzetti F (eds) Geographical information systems in assessing natural hazards. Kluwer Academic Publishers, Dordrecht, pp 93–106
McDermid GJ, Franklin SE (1994) Spectral, spatial, and geomorphometric variables for the remote sensing of slope processes. Remote Sens Environ 49(1):57–71
McDougall S, Hungr O (2005) Dynamic modelling of entrainment in rapid landslides. Can Geotech J 42(5):1437–1448
Meentemeyer RK, Moody A (2000) Automated mapping of conformity between topographic and geological surfaces. Comput Geosci 26(7):815–829
Millington RJ, Quirk JP (1959) Permeability of porous media. Nature 183:387–388
Murali Kumar B (2007) Flood Situation Report—2007 (No—137/2007, 1700 hours, LAST SITREP) disaster management division ministry of home affairs. Government of India, New Delhi
NDM (2009) The Nilgiris—District of Blue Mountains—Schemes—Disaster Management. Nilgiris District Administration, Ooty, India, Government of Tamil Nadu. URL: http://www.nilgiris.tn.gov.in/. Accessed 01 May 2009

Nichol J, Wong MS (2005) Satellite remote sensing for detailed landslide inventories using change detection and image fusion. Int J Remote Sens 26(9):1913–1926

Penman HL (1948) Natural evaporation from open water, bare soil and grass. In: Proceedings of the Royal Society of London, A(194):S120–S145

Ramasamy SM, Francis S, Neelakantan R (2003) Frequent landslides in Nilgiris, India—a phenomenon related to Pleistocene tectonism. In: Ramasamy SM (ed) Remote Sensing Geology. Rawat Publishers Pvt. Ltd., Jaipur, pp 251–255

Rib HT, Liang T (eds) (1978). Recognition and identification: landslides-analysis and control special report, 176, National Academy of Sciences. Transport Research Board, Washington, pp 34–80

Rickenmann D (2005) Runout prediction methods. In: Jacok M, Hungr O (eds) Debris-flow Hazards and Related Phenomena. Springer, Heidelberg, pp 305–321

Sarkar S, Kanungo DP, Patra AK, Kumar P (2008) GIS based spatial data analysis for landslide susceptibility mapping. J Mt Sci 5(1):52–62

Sengupta CK (1995) Detailed study of geofactors in selected hazard prone stretches along the surface communication routes in parts of Darjeeling and Sikkim Himalaya, Phase-I, Part-I (Rongtong-Kurseong road section), Annual progress report (F.S. 1993–94). Geological Survey of India, Government of India

Seshagiri DN, Badrinarayanan S, Upendran R, Lakshmikantham CB, Srinivasan V (1982) The Nilgiri Landslides: results of geotechnical and geological investigations of the G.S.I in collaboration with the state geology branch, government of Tamil Nadu. Miscellaneous Publication No. 57, Geological Survey of India, Government of India, Chennai

Simoni S, Zanotti F, Bertoldi G, Rigon R (2008) Modelling the probability of occurrence of shallow landslides and channelized debris flows using GEOtop-FS. Hydrol Process 22(4):532–545

Skempton AW, DeLory FA (1957) Stability of natural slopes in London Clay. In: 4th International Conference on Soil Mechanics and Foundation Engineering, London, pp 378–381

Soeters R, van Westen CJ (1996) Slope instability. recognition, analysis and zonation. In: Turner AK, Schuster RL (eds), Landslide: investigations and mitigation. Special report 247. Transportation research board. national research council. National Academy Press, Washington, pp 129–177

Sreekumar S (2009) Techniques for slope stability analysis: Site specific studies from Idukki district, Kerala. J Geol Soc India 73(6):813–820

Thakur VC (1996) Landslide hazard management and control in india status report. International Center for Integrated Mountain Development, Kathmandu

Thampi PK, Mathai J, Sankar G, Sidharthan S (1998) Evaluation study in terms of landslide mitigation in parts of Western Ghats, Kerala, Research report submitted to the ministry of agriculture, Government of India. Centre for Earth Science Studies, Government of Kerala, Thiruvananthapuram

van Beek LPH (2002) Assessment of the influence of changes in landuse and climate on landslide activity in a mediterranean environment. PhD Thesis, University of Utrecht, The Netherlands, 363 pp

van Beek LPH, van Asch TWJ (2004) Regional assessment of the effects of land-use change and landslide hazard by means of physically based modeling. Nat Hazards 30(3):289–304

Van Den Eeckhaut M, Reichenbach P, Guzzetti F, Rossi M, Poesen J (2009) Combined landslide inventory and susceptibility assessment based on different mapping units: an example from the Flemish Ardennes, Belgium. Nat Hazards Earth Syst Sci 9(2):507–521

van Westen CJ, Rengers N, Terlien MTJ, Soeters R (1997) Prediction of the occurrence of slope instability phenomena through GIS-based hazard zonation. Geol Rundsch 86(2):404–414

van Westen CJ, van Asch TWJ, Soeters R (2006) Landslide hazard and risk zonation: why is it still so difficult? Bull Eng Geol Environ 65(5):167–184

van Westen CJ, Castellanos E, Kuriakose SL (2008) Spatial data for landslide susceptibility, hazard, and vulnerability assessment: An overview. Eng Geol 102(3–4):112–131

Varnes DJ, IAEG Commission on Landslides and other Mass-Movements (1984) Landslide hazard zonation: review of principles and practice, natural hazards No. 3. UNESCO, Paris, 61 pp

Victor OCD (1962) Kurisumala: A socio-economic survey. St. Joseph's Apostolic Seminary, Alwaye 87 pp

Vinod Kumar K, Martha TR, Roy PS (2006) Mapping damage in the Jammu and Kashmir caused by 8 October 2005 Mw 7.3 earthquake from the Cartosat-1 and Resourcesat-1 imagery. Inter J Remote Sens 27(20):4449–4459

Wieczorek GF (1984) Preparing a detailed landslide-inventory map for hazard evaluation and reduction. Bull Assoc Eng Geol XXI(3):337–342

Wilson RA, Moon AT, Hendickx M (2005) Application of quantitative risk assessment to the Lowrence Hargrave drive project, New South Wales, Australia. In: Hungr O, Fell R, Couture R, Eberhardt E (eds) Landslide risk management. Taylor and Francis Group, London, pp 589–598